CHEMICAL REVIEWS

Review

pubs.acs.org/CR

Mechanisms of Nucleation and Growth of Nanoparticles in Solution

Nguyen T. K. Thanh,* N. Maclean, and S. Mahiddine

Department of Physics and Astronomy, University College London, Gower Street, London, WC1E 6BT, United Kingdom

UCL Healthcare Biomagnetic and Nanomaterials Laboratories, 21 Albemarle Street, London, W1S 4BS, United Kingdom

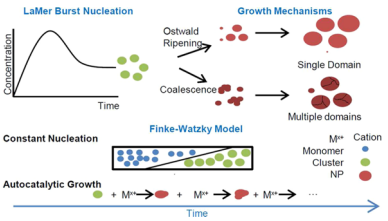

CONTENTS

1. INTRODUCTION

Nanoparticle research has received considerable attention due to many potential innovative applications such as biomedicine,[1,2] catalysis,[3,4] fuel cell,[5] magnetic data storage,[6] agriculture,[7] and solar cells.[8] They have unique and novel magnetic, optical, electronic, and catalytic properties, which are related to their size and are different from bulk materials.

For many years, the process of the nucleation and growth of nanoparticles have been described through the LaMer burst nucleation[9,10] and following Ostwald ripening[11] to describe the change in the particles size. This process was originally modeled by Reiss[12] with an accepted model being developed by Lifshitz–Slyozov–Wagner, LSW theory.[13,14] This was considered to be the only theory of nucleation until Watzky and Finke[15] formulated an approach of constant slow nucleation followed by autocatalytic growth. The elucidation of these mechanisms was possible thanks to in- and ex-situ measurements. UV–vis spectroscopy is very common technique to determine the particle size of quantum dot based on empirical formulas.[16−23] In a more recent study, with the use of small-angle X-ray scattering (SAXS) and a liquid cell within a transmission electron microscope (TEM), it has been possible to further probe nanoparticles in situ and obtain detailed information on how nanoparticles growth in solution.[24] Recent reviews have covered different processes of the nucleation and growth of nanoparticles from solution,[25−27] vapor,[28] or epitaxial growth.[29] This review presents some of the most recent analyses showing how noble metals, quantum dots, and magnetic nanoparticles nucleate and grow in solution.

2. CLASSICAL NUCLEATION AND GROWTH

2.1. Classical Nucleation

Nucleation is the process whereby nuclei (seeds) act as templates for crystal growth. Primary nucleation is the case of nucleation without the presence of other crystalline matter as defined by Mullin.[30] This can be used to describe the nucleation of many chemical syntheses.[31,32] However, the formation of porous solids does not always follow the classical pathways of crystallization in solution. Furthermore, Habraken et al.[33] demonstrate that ion-association complexes unite classical and nonclassical theories for the biomimetic nucleation of calcium phosphate. Homogeneous nucleation occurs when nuclei form uniformly throughout the parent phase, whereas, heterogeneous nucleation forms at structural inhomogeneities (container surfaces, impurities, grain boundaries, dislocations). In liquid phase, heterogeneous occurs much easier, since a stable nucleating surface is already present. The process of homogeneous nuclei formation can be considered thermodynamically[25,30] by looking at the total free energy of a nanoparticle defined as the sum of the surface free energy and the bulk free energy. For a spherical particle of radius r, the surface energy γ and the free energy of the bulk crystal ΔG_v, giving a total free energy ΔG, eq 1.

The crystal free energy itself, ΔG_v is dependent upon the temperature T, Boltzmann's constant k_B, the supersaturation of the solution S, and its molar volume, v. ΔG_v is defined in eq 2.

$$\Delta G = 4\pi r^2\gamma + \frac{4}{3}\pi r^3 \Delta G_v \quad (1)$$

Received: October 14, 2013

   dx.doi.org/10.1021/cr400544s | Chem. Rev. XXXX, XXX, XXX–XXX

$$\Delta G_v = \frac{-k_B T \ln(S)}{v} \quad (2)$$

Due to the surface free energy always being positive and the crystal free energy always being negative, it is possible to find a maximum free energy which a nucleus will pass through to form a stable nucleus by differentiating ΔG with respect to r and setting it to zero, $d\Delta G/dr = 0$, which gives a critical free energy, eq 3. By the way, the critical radius is defined in eq 4:

$$\Delta G_{crit} = \frac{4}{3}\pi\gamma r_{crit}^{\ 2} = \Delta G_{crit}^{homo} \quad (3)$$

$$r_{crit} = \frac{-2\gamma}{\Delta G_v} = \frac{2\gamma v}{k_B T \ln S} \quad (4)$$

This critical radius corresponds to the minimum size at which a particle can survive in solution without being redissolved. The same is true for the particle's free energy, where a critical free energy is required to obtain stable particles within solution, Figure 1.

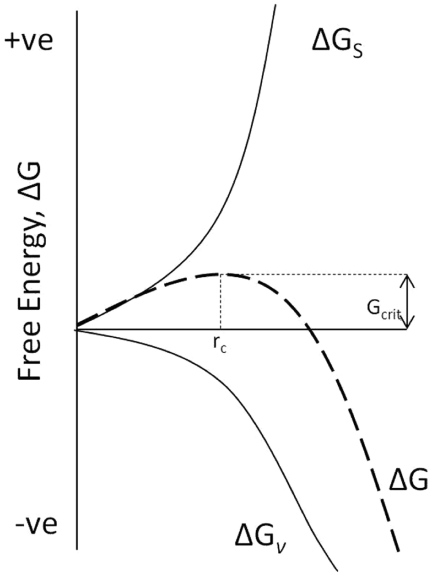

Figure 1. Free energy diagram for nucleation explaining the existence of a "critical nucleus."

A rate of nucleation of N particles during time t can be described using an Arrhenius type equation, eq 6, where A is a pre-exponential factor.

$$\frac{dN}{dt} = A \exp\left(-\frac{\Delta G_{crit}}{k_B T}\right) \quad (5)$$

$$\frac{dN}{dt} = A \exp\left(\frac{16\pi\gamma^3 v^2}{3k_B^{\ 3}T^3(\ln S)^2}\right) \quad (6)$$

From eq 6, three experimental parameters can be varied: supersaturation, temperature, and the surface free energy. Kwon and Hyeon[25] plotted these three parameters, Figure 2. The largest effect on nucleation rate comes from supersaturation, where a change from $S = 2$ to $S = 4$ causes an increase in the nucleation rate about $\sim 10^{70}$, and a variation in the surface free energy caused by different surfactants.

Often, especially in industrial environments, the solutions can contain impurities of another phase. In the presence of active centers (impurities, walls, bubbles, drops, etc.), the barrier to overcome for nucleation to occur is globally decreased. Unlike homogeneous nucleation, the nuclei are formed on the first surface of a foreign body. Germs that thrive on support surfaces no longer have the spherical shape (assumption of classical nucleation theory), but caps forming a spherical contact angle θ with the support, Figure 3. If $\theta \leq \pi$,

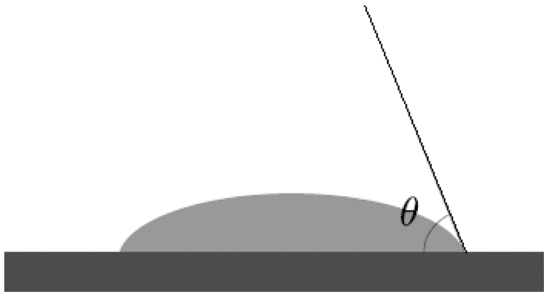

Figure 3. Illustration of the contact angle θ for the heterogeneous nucleation.

nuclei and active centers have a high affinity. The surface term is strongly decreased, Figure 1. To account for these phenomena, a correction term is introduced into the law of homogeneous primary nucleation,[34] so the free energy needed for heterogeneous nucleation is equal to the product of homogeneous nucleation and a function of contact angle, eq 7.

$$\Delta G_{crit}^{hetero} = \phi \Delta G_{crit}^{homo} \quad (7)$$

ϕ is a factor dependent on the contact ongle θ, with

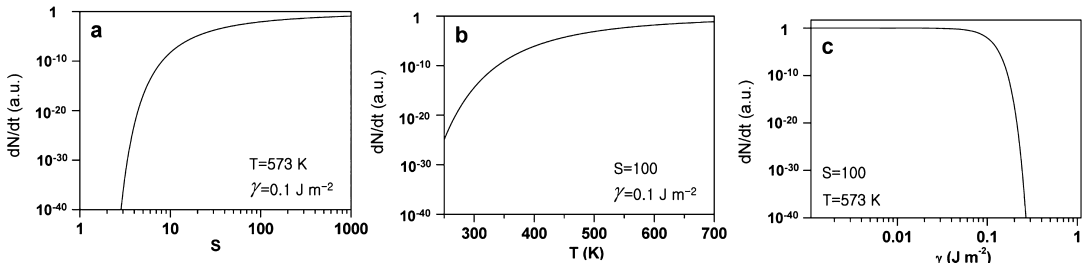

Figure 2. Nucleation rate as a function of a) supersaturation, b) temperature, and c) the surface free energy calculated using eq 6. v is set as 3.29×10^{-5} m^3 mol^{-1}, the value for CdSe. The nucleation rate is normalized with the pre-exponential factor A. Reprinted with permission from ref 25. Copyright 2011 WILEY-VCH Verlag GmbH & Co. KGaA, Weinheim.

dx.doi.org/10.1021/cr400544s | Chem. Rev. XXXX, XXX, XXX–XXX

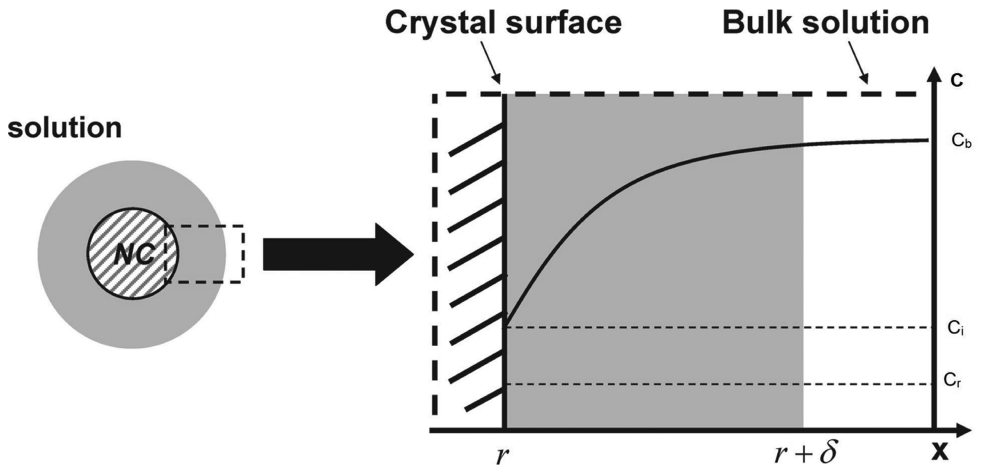

Figure 4. Schematic illustration of diffusion layer structure near the surface of a nanocrystal (left) and plot for the monomer concentration as a function of distance x (right). The shaded area indicates the diffusion layer. Reprinted with permission from ref 25. Copyright 2011 WILEY-VCH Verlag GmbH & Co. KGaA, Weinheim.

$$\phi = \frac{(2 + \cos\theta)(1 - \cos\theta)^2}{4} \tag{8}$$

2.2. Classical Growth

The growth of nanoparticles is dependent on two mechanisms: the surface reaction and the monomer's diffusion to the surface.[35] To model growth by diffusion Fick's first law, eq 9 can be applied, where r, J, D, and C are respectivelly the particle radius, the total flux of monomers passing through a spherical plane with radius x, the diffusion coefficient and the concentration at a distance x, Figure 4.

$$J = 4\pi x^2 D\frac{dC}{dx} \tag{9}$$

Fick's first law can be rewritten, eq 10, for the case of a nanoparticle within solution where δ is the distance from the particle surface to the bulk concentration of monomers within solution, C_b is the bulk concentration of monomers within the solution, C_i is the concentration of monomers at the solid/liquid interface, and C_r is the solubility of the particle, Figure 4.

$$J = \frac{4\pi Dr(r + \delta)}{\delta}(C_b - C_i) \tag{10}$$

As J is constant irrespective of x due to the steady state of the solute diffusion, integration of $C(x)$ from $(r + \delta)$ to r gives eq 11:

$$J = 4\pi Dr(C_b - C_i) \tag{11}$$

A similar equation can be written for the rate of surface reaction "k", eq 12. The rate of the surface reaction is assumed to be independent of particle's size.

$$J = 4\pi r^2 k(C_i - C_r) \tag{12}$$

From eqs 11 and 12 there are two limiting factors: either the diffusion of monomers to the surface or the rate of reaction of these monomers on the surface. If diffusion is the limiting factor then the change in particle size with time is given by eq 13:

$$\frac{dr}{dt} = \frac{Dv}{r}(C_b - C_r) \tag{13}$$

Similarly if the surface reaction is the limiting factor then eqs 11 and 12 can be approximated to eq 14.

$$\frac{dr}{dt} = kv(C_b - C_r) \tag{14}$$

When the growth of nanoparticles is neither diffusion nor surface reaction controlled, the increase in particle's radius with time is written as eq 15:

$$\frac{dr}{dt} = \frac{Dv(C_b - C_r)}{r + D/k} \tag{15}$$

Strictly speaking, the solubility of nanoparticles is not independent of particle's size and according to Gibbs–Thomson relation, eq 16, a spherical particle has an extra chemical potential $\Delta\mu = 2\gamma v/r$. Then C_r is expressed as a function of r where v is the molar volume of the bulk crystal and C_b is the concentration of the bulk solution.

$$C_r = C_b \exp\left(\frac{2\gamma v}{rk_BT}\right) \tag{16}$$

For the growth of NPs, a general expression 13 can be produced through combining eqs 17 and 15.[37,38]

$$\frac{dr^*}{d\tau} = \frac{S - \exp\left(\frac{1}{r_{cap}}\right)}{r_{cap} + K} \tag{17}$$

where the three dimensionless constants are defined as follows:

$$r_{cap} = \frac{RT}{2\gamma v}r \tag{18}$$

$$\tau = \frac{k_B{}^2T^2DC_b}{4\gamma^2 v}t \tag{19}$$

$$K = \frac{k_BT}{2\gamma v}\frac{D}{k} \tag{20}$$

Within eqs 19 and 20, $2\gamma v/k_BT$ is the capillary length and K is the Damköhler number. The Damköhler number indicates whether the reaction is diffusion or reaction rate dependent. If

dx.doi.org/10.1021/cr400544s | Chem. Rev. XXXX, XXX, XXX–XXX

$D \ll 1$ then the diffusion rate dominates over the surface reaction.

More details of the mathematical aspect of the above theory on growth of nanocrystals in solution was described elsewhere.[36]

2.3. Formation of a Size Distribution

The previous sections have led to the same conclusion: above some critical radius, the particles will form and grow whereas below this radius, the particles will redissolve. This, however, does not explain the differences in the sizes of the particles during growth. There is a size focusing effect called Ostwald ripening which can be taken into account by looking at the diffusion controlled growth and rewriting eq 13 using eq 16, where r^* is the particle radius in equilibrium within the bulk solution.

$$\frac{dr}{dt} = \frac{K_D}{r}\left(\frac{1}{r^*} - \frac{1}{r}\right) \tag{21}$$

where K_D is defined as follows:

$$K_D = \frac{2\gamma D v^2 C_b}{k_B T} \tag{22}$$

If the size distribution is narrow, the change in the standard deviation, Δr for a given particle radius at equilibrium is given by eq 23.

$$\frac{d(\Delta r)}{dt} = \frac{K_D \Delta r}{\bar{r}^2}\left(\frac{2}{\bar{r}} - \frac{1}{r^*}\right) \tag{23}$$

where $\bar{r}$ is the mean particle radius. For eq 23 there are two regimes depending on the supersaturation. If the supersaturation is high such that $\bar{r}/r^* \geq 2$ then $d(\Delta r)/dt \leq 0$ and the growth of the system is self-sharpening of the size distribution. However, if $\bar{r}/r^* < 2$ then $d(\Delta r)/dt > 0$ and then the size distribution tends to broaden even within the diffusion controlled growth.

Similarly there are a set of equations for surface reaction controlled growth: eq 24 where K_R is given by eq 25 and the change in standard deviation with time is given by eq 26.

$$\frac{dr}{dt} = K_R\left(\frac{1}{r^*} - \frac{1}{r}\right) \tag{24}$$

$$K_R = \frac{2\gamma k v^2 C_b}{RT} \tag{25}$$

$$\frac{d(\Delta r)}{dt} = \frac{K_R \Delta r}{\bar{r}^2} \tag{26}$$

In the case where the surface reaction dominates, the size distribution will allways be within the broadening regime, this is as for any value of $\bar{r}$, $d(\Delta r)/dt$ will always be positive and this is due to the Gibbs–Thomson relation, eq 16. Within the diffusion controlled growth regime, as time increases, the Gibbs–Thomson effect relating the solubility of a particle to its size which becomes negligible and the self-sharpening of the size distribution becomes iron carboxylate first then to $\bar{r}$ is around $1r^* - 3r^*$ which is clearly visible in Figure 5 solid line.

Furthermore, across all values of r^* above 1, the value of $1/K_D\ d\bar{r}/dt$ is positive, and this is indicative of a self-sharpening regime of growth. However, this self-sharpening effect becomes negligible as the particle size increases.

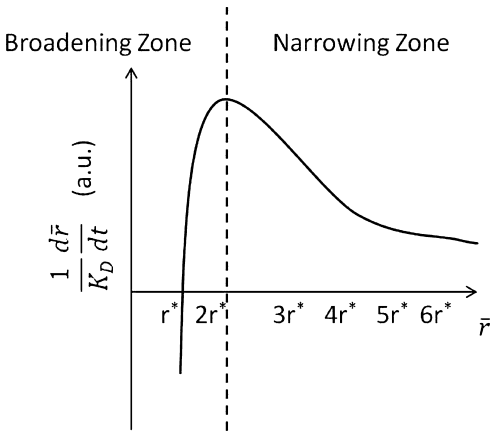

Figure 5. Schematic of $[d\bar{r}/dt]/K_D$ as a function of $\bar{r}$ for diffusion-controlled growth within an infinite diffusion layer showing how above $2r^*$ the size distribution narrows within increasing size.

3. THEORIES OF NUCLEATION AND GROWTH

Within this section we shall highlight the different theories for the nucleation and growth of nanoparticles (NPs) outlining what occurs within the different processes.

3.1. LaMer Mechanism

The first mechanism was the LaMer mechanism[9,10] which has the conceptual separation of the nucleation and growth into two stages. LaMer studied the synthesis of sulfur sols from the decomposition of sodium thiosulfate, consisted in two steps: the first to form free sulfur from the thiosulfate and the second form sulfur sols in solution. The process of nucleation and growth through the LaMer mechanism can be divided into three portions. (I) A rapid increase in the concentration of free monomers in solution, (II) the monomer undergoes "burst-nucleation" which significantly reduces the concentration of free monomers in solution. The rate of this nucleation is described as "effectively infinite" and after this point, there is almost no nucleation occurring due to the low concentration of monomers after this point; (III) following nucleation growth occurs under the control of the diffusion of the monomers through the solution. The three stages are shown in Figure 6 where the concentration of the monomers is schematically plotted as a time's function. A good example of this, is the growth of silver halides which have been studied in depth and follow this classical nucleation and growth.[39,40]

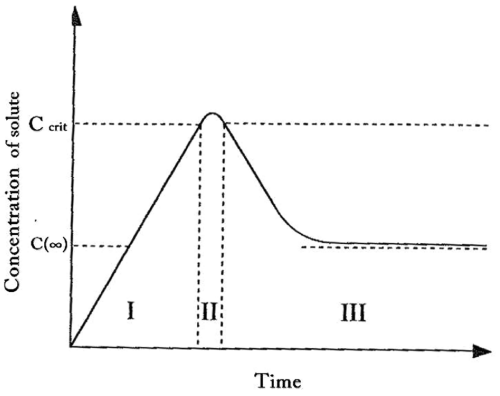

Figure 6. LaMer diagram schematic. Reprinted with permission from ref 41. Copyright 2007 Elsevier.

dx.doi.org/10.1021/cr400544s | Chem. Rev. XXXX, XXX, XXX–XXX

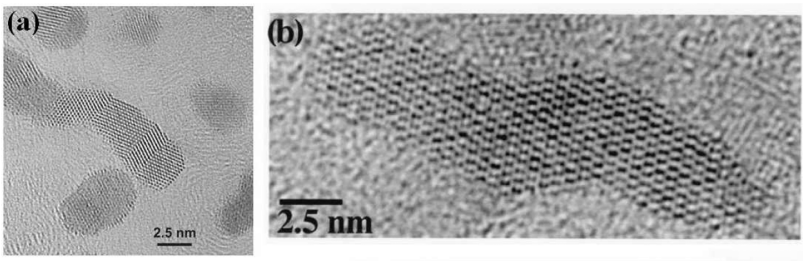

Figure 7. (a) Coalescence of platinum crystallites has led to this platinum nanowire. (b) A formation of four titania crystallites forming one large crystallite through orientated attachment. Reproduced with permission from ref 48. Copyright 1999 Elsevier.

3.2. Ostwald Ripening and Digestive Ripening

Ostwald ripening[11] was first described in 1900. The mechanism of growth is caused by the change in solubility of NPs dependent on their size which is described by the Gibbs–Thomson relation, eq 16. Due to the high solubility and the surface energy of smaller particles within solution, these redissolve and in turn allow the larger particles to grow even more. The mathematical theory of Ostwald ripening within a close system is described by Lifshitz and Slyozov[13] and Wagner.[14]

Digestive ripening is effectively the inverse of Ostwald ripening. Within this case, smaller particles grow at expense of the larger ones and has been described by Lee et al.[42] where an applicable form of the Gibbs–Thomson equation, eq 16, is derived. This process of formation is controlled once again by the surface energy of the particle within solution where the larger particle redissolve and in turn smaller particles grow.

3.3. Finke-Watzky Two Step Mechanism

The Finke-Watzky two step mechanism is a process of nucleation and growth where both steps happen simultaneously.[15] The first is a slow continuous nucleation, eq 27 and the second is the autocatalytic surface growth which is not diffusion controlled, eq 28.

$$A \rightarrow B \tag{27}$$

$$A + B \rightarrow 2B \tag{28}$$

This process was discovered through the reduction of a transition metal salts by hydrogen which was studied by following the reduction of cyclohexene. Currently, this method is shown through the kinetic fitting of the cyclohexene reduction and has not been proven explicitly. Although, this method is different from classical nucleation, the nucleation step still follows a critical size described within a classical nucleation framework.

This has been shown to be a good fit for many systems including iridium,[15,43] platinum,[44] ruthenium[45] and rhodium.[45]

3.4. Coalescence and Orientated Attachment

Coalescence and orientated attachment are very similar. However, they differ in the orientation of the crystal lattice at the grain boundary. For the coalescence, there is no particular preference for the attachment[24] whereas for the orientated attachment, there is a common crystallographic alignment of the attachment to occur, which is allowing for continuous crystallographic planes.[46] Figure 7 shows nanoparticles which have undergone (a) coalescence and (b) orientated attachment. It is hard to see from these high resolution images that within coalescence the lattice planes are randomly orientated between domains whereas for orientated attachment there is a perfect alignment of the planes.

One of the most recent study on orientated attachment was carried out by Li et al.[47] where the orientated attachment of iron oxyhydroxide has been viewed in real time using a liquid cell within a high resolution transmission electron microscope (HRTEM). It was found that particles will rotate and have contact with each other until the crystallographic orientation of the two crystals matched or until a twin match. Following the attachment, the space between the particles was filled on the order of 10 to 100 s. To make this contact the particles were seen to 'jump' in the range of 0.5–1 nm, and it has been suggested that this attraction is Coulombic in nature. However, van der Waals interactions with anisotropic polorisability can not be ruled out.

3.5. Intraparticle Growth

Intraparticle ripening as described by Peng et al.[49,50] is the diffusion of monomers along the surface of a nanomaterial to change the shape of the particle with time. This case occurs under very specific conditions where the energy of monomers within solution is lower than the one of the crystal facets of the nanoparticles. This means that the surface energy of the particle is almost equal to the bulk solution one and in this case there would be no net diffusion: with no adding in flux of monomers onto the particle's surface. The only instability within the system is the surface energy of the different facets of the particle itself. In this case the high energy facets dissolve and the low one will grow leading to an apparent intraparticle diffusion.

4. NOBLE MATERIALS

4.1. Gold

Gold colloids were synthesized even back to 1857 by Faraday.[51] Since then, there have been numerous studies trying to understand the nucleation and growth of the particles including Turkevich[52] and Rothenberg et al.[53]

Rothenberg's study used UV–visible spectroscopy to allow the formation of gold nanoparticles within solution to be tracked. Whereas in recent times, X-ray spectroscopies have been used to monitor the growth of gold nanoparticles.[54,55]

Ji et al.[56] have shown that the pathway, whereby the gold particles synthesized vary depending on pH, with the particle growth following one of two pathways. The method follows the general synthesis set out by Turkevich: injecting trisodium citrate into a boiling solution of tetrachloroauric acid.[52] However, with the additional changes made by Fren[57] where the pH is controlled by the concentration of trisodium citrate. For a low pH, pH 3.7–6.5, the particles form through an intermediate of $[AuCl_3(OH)]^-$ which undergoes nucleation within 10 s, a LaMer burst nucleation, followed by fast random attachment and finally intraparticle ripening. For a higher pH ~6.5–7.7, the particles undergo reduction through [Au-

dx.doi.org/10.1021/cr400544s | Chem. Rev. XXXX, XXX, XXX–XXX

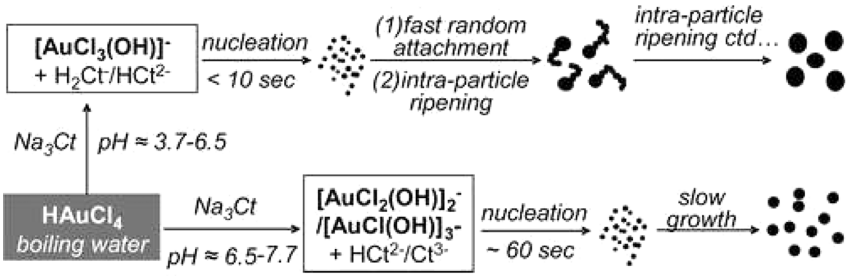

Figure 8. Schematic illustration of two reaction pathways for the formation of gold nanoparticles by citrate reduction. Reprinted with permission from ref 56. Copyright 2007 American Chemical Society.

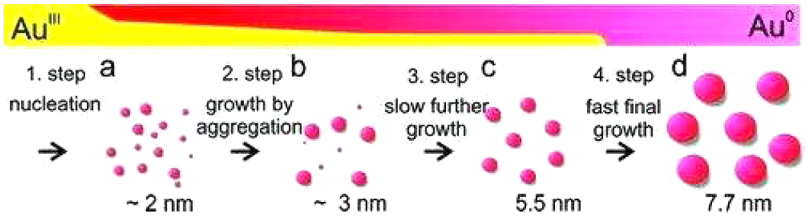

Figure 9. Schematic illustration for the deduced process of gold nanoparticle formation. Reprinted with permission from ref 60. Copyright 2010 American Chemical Society.

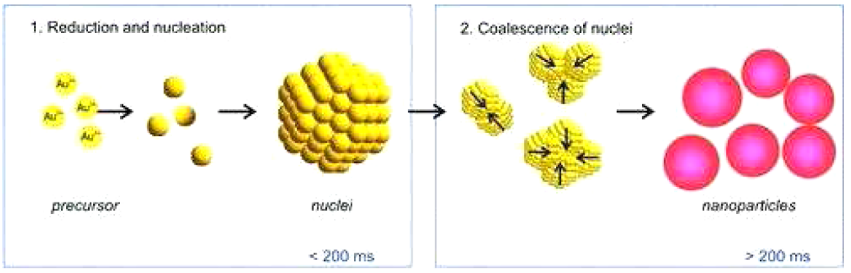

Figure 10. Schematic illustration of the formation of gold nanoparticles. Reprinted with permission from ref 63. Copyright 2010 American Chemical Society.

$Cl_2(OH)]_2^-$ and $[AuCl(OH)]_3^-$ with a much longer nucleation of ~60 s followed by slow growth, Figure 8.

Within the synthesis of gold nanoparticles, it is somewhat unclear which chemical reaction is occurring and there are two separate pathways which the gold could undertake. The first is to bond as ions then a reduction to occur, eq 29 or for the reduction to occur first and then a bonding of the gold atoms, eq 30.[58]

$$M^{x+} + xe \rightarrow M^0$$
$$M^0 + M_n^0 \rightarrow M_{n+1}^0 \quad (29)$$

$$M^{x+} + e \rightarrow M^{(x-1)+}$$
$$M^{(x-1)+} + M^{(x-1)+} \rightarrow M_2^{(2x-2)+}$$
$$M_2^{(2x-2)+} + xe \rightarrow M_x \quad (30)$$

The fast random attachment within the Turkevich synthesis was further researched by Pong et al.,[59] where chains of Au particles were observed through TEM and UV−vis spectroscopy. These chains which were previously unseen were discovered to undergo fragmentation and following Ostwald ripening to form spherical gold particles. Pong et al. were also able to observe these chains when using $HAuCl_4$ and sodium borohydride, $NaBH_4$. However, with the strong reducing agent $NaBH_4$ the transient state is too short-lived to isolate them from the reaction solution.

Polte et al.[60] have studied the case where the reaction was carried out within a batch reactor and samples were extracted, then measured by X-ray absoption near edge structure (XANES), SAXS, and UV−visible spectroscopy. The reaction was carried out using tetrachloroauric acid in water at different temperatures and injecting trisodium citrate. This has shown another stage of growth of gold nanoparticles within aqueous solution.

Figure 9 shows the formation of the particles deduced by Polte, where a four-step process has been determined. The first step of the process is considered to be nucleation where 20% of the initial gold salt forms particles within the first 20 s. The average particle radius is less than 2 nm, which then undergo coalescence within 20 min to form 4 nm mean radius particles with a polydispersed sample of about 45%. The growth from 2 to 4 nm is thought to occur through either Ostwald ripening[61] or coalescence.[62]

The second step is the growth of the particles up to an average size 5.2 nm where the dispersity of the sample reduces significantly in line with self-sharpening growth by diffusion. However, diffusion controlled growth usually only occurs over a few seconds, in this case it occurs during 25 to 50 min. The reason behind this long diffusion controlled growth time is due to the constant reduction of gold that occurs within the

dx.doi.org/10.1021/cr400544s | Chem. Rev. XXXX, XXX, XXX−XXX

solution where the limiting factor is the concentration of gold metal within the solution itself.

The fourth step is a rapid consumption of the gold salt left in solution where the particle size increases rapidly from 5.2 to 7.7 nm with a decrease in the polydispersity to 10% observed from 50 to 70 min within solution. This is considered to be an autocatalytic reduction on the surface of the nanoparticles.

A further study by Polte et al.[63] used a static mixer in continuous flow reducing tetrachloroauric acid with sodium borohydride a strong reducing agent with analysis from SAXS, UV−vis and XANES. Within this case, the reduction of a gold salt and nucleates in less than 200 ms which is the resolution limit for a SAXS data to measure, from here coalescence occurs which is measured through a rapid reduction in the number of particles within solution measured though SAXS, Figure 10. Due to the lack of any stabilizing agent with the solution, usually citrate, the growth continued even 24 h after the starting point.

A follow up study was carried out by Polte et al.[64] confirming the autocatalyic growth of gold nanoparticles, showing that an addition of a gold salt to gold seeds will cause a reduction of gold salt with an increase in particle size.

Mikhlin et al.[65] studied the reduction of tetrachloroauric by trisodium citrate in the presence of sodium hydroxide. Within these experiments, Mikhlin heated a solution of gold salt and injected the citrate and sodium hydroxide at 70 °C. Then following this, the reaction was quickly stopped by cooling the solution to room temperature rapidly then analyzed using AFM, SAXS and UV−vis spectroscopy, with the AFM being carried out on a dry sample. It was discovered that the solution appears to form droplets with small conduits in between. These results agree with those of Polte[60] which show coalescence of 1−2 nm particles within solution. It is thought that the droplets of reduced species may aid the coalescence of the initial gold particles. This work also agrees with that of Polte, which indicates that the limiting factor is the reduction of gold ions to form gold metal within solution, Figure 11.

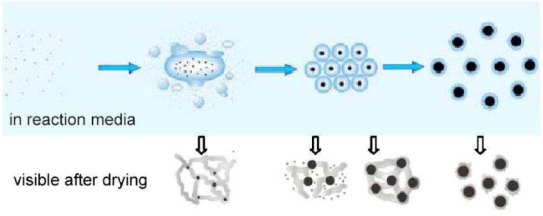

Figure 11. Schematic illustration of the formation of gold nanoparticles studied using AFM. Reprinted with permission from ref 65. Copyright 2011 Elsevier.

Coalescence has also been observed by Shields et al.[66] in the formation of thiolated gold particles through the reduction of tetrachloroauric acid by sodium borohydride in toluene in the presence of tetraoctylammonium bromide, TOABr, and decanethiol at 180 °C. This process was shown to grow under coalescence and following this undergo Ostwald ripening proven by using HRTEM.

Figure 12 shows domains about 1.5 nm in size, and a total gold particle size of 4 nm. This confirms the coalescence theory, as the particles before coalescence are about 1.5 nm and form 8 domains within a particle of 4 nm. If growth was from purely Ostwald ripening, then only one crystal domain would appear. It was also found to be a bimodal size distribution,

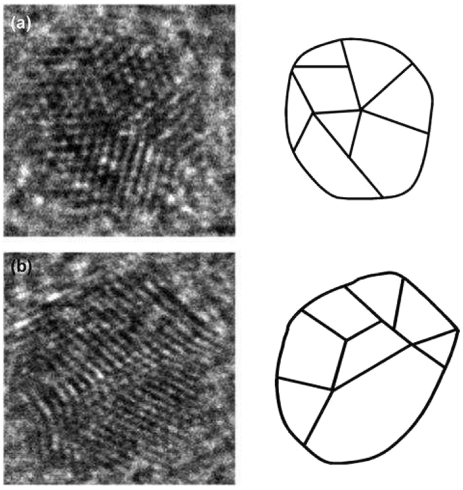

Figure 12. HRTEM image of polycrystalline gold. Reprinted with permission from ref 66. Copyright 2010 American Chemical Society.

which is highly indicative of coalescence, and bimodal size distribution is present until Ostwald ripening takes over as the major growth mechanism with time.

The nucleation process of gold has also been investigated in the reaction of auric acid, citric acid, and poly(vinylpyrrolidone), PVP, in water at 70 °C within a batch reactor. The process of nucleation was investigated by Yao et al.[58] using X-ray absorption fine structure, XAFS, looking at the bonding between gold atoms. The ideal theoretical calculated gold bond length is within the range of 2.55−2.70 Å for gold nanoparticles which is much shorter than the bulk bond length of 2.87 Å. The bond length when measured through XAFS was found to be 2.92 Å which is larger than both bulk and nanoparticle, and this is due to the charge transfer from the Cl to the Au atoms. As the reaction proceeds, the bond length decreases to below that of the bulk to that of a nanoparticle due to the increase in particle size which decreases the surface area per gold atom and the effectient coverage of Cl ions. The competition between particle size and ligand binding effect leads to a smaller bond size than the bulk. Within this particular case with the PVP present, there is the formation of Au_2Cl_6 dimers which then go on to form trimers. Following this, there is a reduction process which occurs leading to the formation of gold clusters such as Au_{13} with the surface atoms as chlorinated gold ions. This then leads to a final step where larger clusters form through coalescence which is represented in Figure 13.

4.2. Silver

The formation mechanism behind silver nanoparticles has been studied in depth under various conditions and these were first studied by Rothenberg et al.[53] To further understand the mechanisms of silver nucleation and growth, γ-irradiation of silver perchlorate, $AgClO_4$, in the presence of propanol, N_2O, and sodium citrate was studied by Henglein.[67] A low concentrations of citrate lead to particle coalescence as a major growth pathway, whereas at higher citrate concentrations the growth occurred through the reduction of silver ions on the surface of the particles.

Henglein et al. propose two mechanisms of silver NP growth, Figure 14. Surface reduction growth which leads to monodisperse particles occurs via electron transfer which reduces Ag^+ ions onto the surface of the particles which are already present in the solution. The study suggests that if the

dx.doi.org/10.1021/cr400544s | Chem. Rev. XXXX, XXX, XXX−XXX

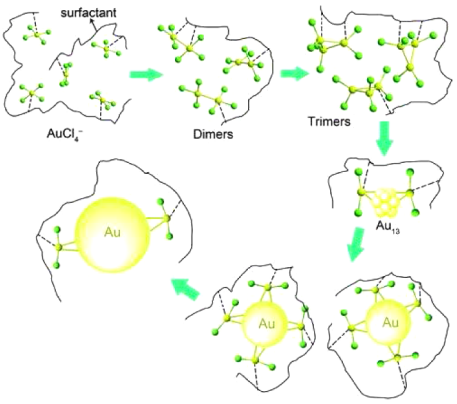

Figure 13. Formation of gold nanoparticles through Au_2Cl_6. Reprinted with permission from ref 58. Copyright 2010 American Chemical Society.

citrate concentration is too low, the silver NPs are not sufficiently covered with stabilizing citrate and coalescence occurs.

At higher concentrations, the ionic strength of the solution destabilizes particles. A very important growth experiment carried out which involved taking a seed solution of silver NPs and adding further silver precursor and reducing electrons to check how the seed particles were affected. The experiment shows a perfect surface reduction occurring as all the silver reduces to make existing particles bigger rather than produce new particles. This occurs by introducing 5 mL of seed particles to another 35 mL of solution, which after irradiation produces particles which have grown perfectly in size according to the amount of silver added. This is important because it shows the potential for tuning NP sizes but more importantly that the mechanism of surface reduction for growth of silver NPs exist.

In more recent time with the introduction of SAXS, Harada and Katagiri[68] investigated the photoreduction of silver perchlorate hydrate in the presence of poly(*N*-vinyl-2-pyrrolidone), PVP, with benzoin as the photoactivator in a 1:1 ethanol:water solution. The reaction was followed using UV−vis spectroscopy and in situ SAXS. The formation of the silver particles were found to be formed through 2 phases: the first phase is an initiation stage where, a rapid increase in the number of Ag particles in solution within the first 10 min occurs. There is a combination of both nucleation and reduction of Ag^+ ions to Ag^0 with a large polydispersity of about 20%. This was the first phase and was found to be an autocatalytic reduction--nucleation which is the two-step mechanism proposed by Finke and Watzky.[43] In the second phase there is a notable decrease in the number of particles while simultaneously there is an increase in the particle size which can be directly explained through Ostwald ripening and also the data is in excellent agreement with Lifshitz−Slyozov−Wagner, LSW theory.[13,14]

For the lowest concentration of silver 5 mM there is a third stage which occurs over 30−90 min where the particle radius increases but within this case the model that fits is the dynamic coalescence of particles within solution. To further investigate this third phase, the particle size distribution was observed at different time periods. From 50 to 85 min, distributions are of interest as they could indicate where the silver changes from Ostwald ripening to coalescence. The distributions were fitted to a Wagner-type Ostwald ripening model showing that there is a transient regime from Ostwald ripening growth to coalescence based growth.[69−71] Although the distributions show a skew to larger sizes which does not mean that Ostwald ripening can be ruled out due to the modified LSW models.[72,73] Figure 15a. This matches extremely well with the TEM results from this 5 mM experiment where the size distribution. Figure 15b shows the same shape of distribution.

From all of this work Harada formed the following mechanism for the photoreduction of silver, Figure 16.

Richards et al.[74] used $[(PPh_3)_2Ag(O_2CC_{13}H_{27})]$ as a method of tracking the reaction through three separate channels, the first is UV−vis spectroscopy through the surface plasmon resonance of the silver particles, second is by monitoring $^{31}P^1H$ NMR and third through taking samples with time and viewing them under the TEM. The reaction mixture consisted of the silver precursor, azobis(isobutyronitrile) (AIBN), at 130 °C in poly(1-hexadecene)$_{0.67}$-*co*-(1-vinylpyrrolidone)$_{0.33}$. The key data is contained within the TEM particle size distribution analysis which were shown to be asymptotic at first then changes to bimodal with time. This can not be explained by Ostwald ripening as a growth mechanism, Figure 17. Also Figure 17 shows that under HRTEM, the particles are

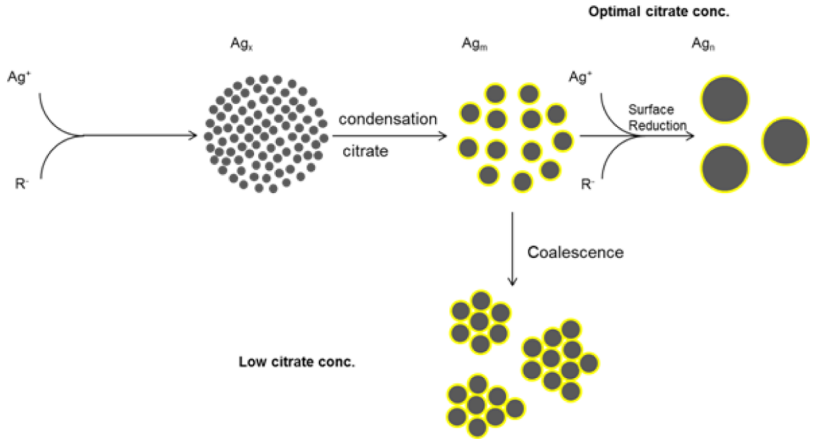

Figure 14. Growth mechanisms proposed by Henglein at low and optimal citrate concentrations with two different mechanisms occurring. At optimal concentrations, it is suggested that a surface reduction of silver ions occurs on the surface of formed NPs owing to the reduction potential of the citrate adsorbed onto the surface. At low concentrations, coalescence of smaller silver NP clusters occurs. Adapted with permission from ref 67. Copyright 1999 American Chemical Society.

dx.doi.org/10.1021/cr400544s | *Chem. Rev.* XXXX, XXX, XXX−XXX

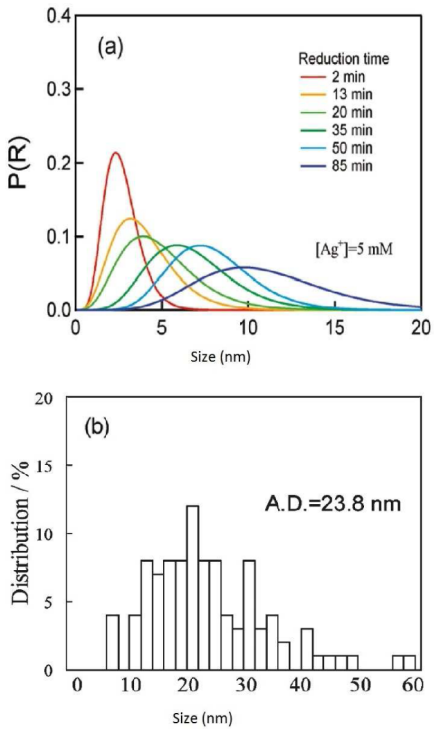

Figure 15. Predicted particle size distributions from SAXS of [Ag] = 5 mM at a series of times. Reprinted with permission from ref 68. Copyright 2010 American Chemical Society.

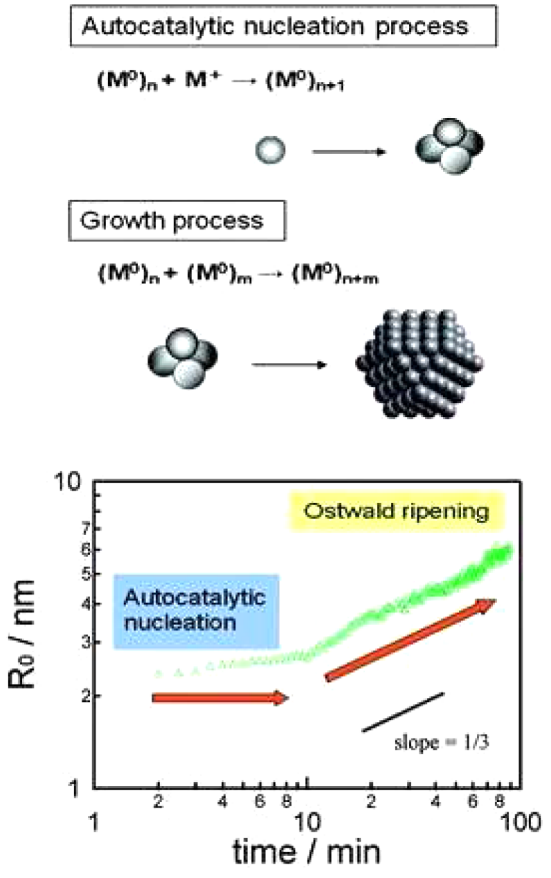

Figure 16. Change in particle radius and the proposed mechanism for the formation of silver nanoparticles. Reprinted with permission from ref 68. Copyright 2010 American Chemical Society.

polydispersed which is an indication of aggregative or coalescent growth.

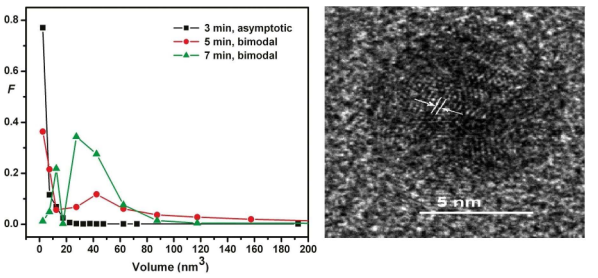

Figure 17. Plots show the evolution of the particle size distributions from asymptotic to bimodal. The fraction F of the nanoparticles in a given volume bin is plotted against nanoparticle volume. Reprinted with permission from ref 74. Copyright 2010 American Chemical Society.

Looking at the kinetics of this particle growth which is considered to be coalescence, would follow a sigmoidal growth profile.[27,37,44,75,76] The growth of these silver nanoparticles follows this sigmoidal growth pattern until Ostwald ripening occurs causing a linear growth pattern, Figure 18.

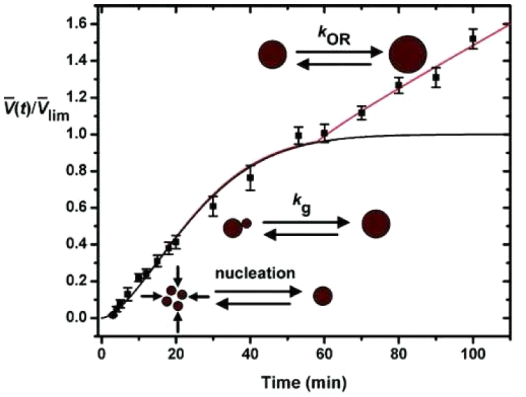

Figure 18. Plot of the growth of particle size with time showing the graph for a sigmoidal curve using V_{lim} is the mean volume at the end of coalescent growth before Oswald ripening takes over in the linear region. Reprinted with permission from ref 74. Copyright 2010 American Chemical Society.

Within this case, there is a three-step process: the nucleation is considered to follow the LaMer mechanism, burst nucleation; following this there is coalescent growth which accounts for both the bimodal size distribution and the polycrystalline particles which were observed through the TEM. Following this coalescent process, an Ostwald ripening is observed which corresponds to the linear portion above 60 min reaction time, Figure 18.

Furthering this coalescent growth Takesue et al.[77] carried out SAXS on the synthesis of silver nanoparticles where silver nitrate was reduced by sodium citrate and tannic acid in water which had its pH adjusted to 12 with sodium hydroxide. By using of SAXS reaction times of 0.18−0.98 ms were probed. The first 0.39 ms is described as an induction period where the reduction of the silver nitrate starts but nucleation has not yet occurred. Between 0.39 and 0.59 ms there is some form of nucleation however the particle size is too small for the SAXS to detect. From 0.59 to 0.79 ms peaks could be detected at sizes

dx.doi.org/10.1021/cr400544s | Chem. Rev. XXXX, XXX, XXX−XXX

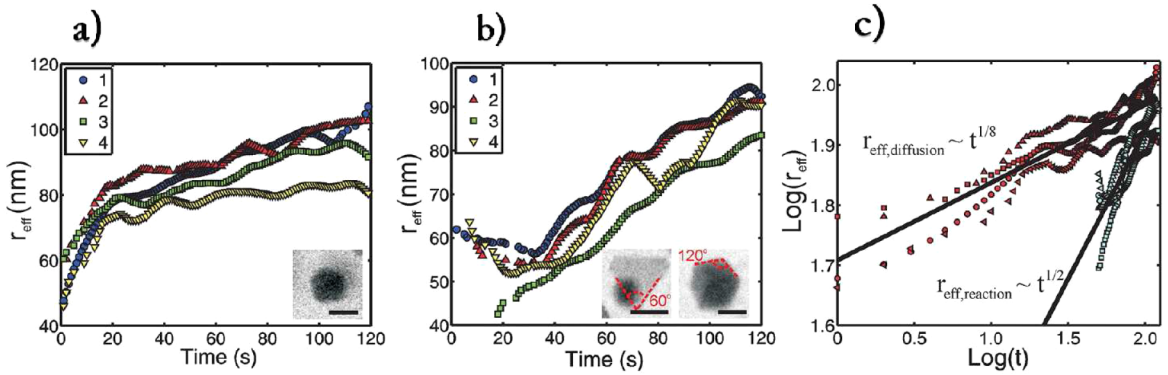

Figure 19. (a) Plot of the effective radius (r_{eff}) as a function of time for four individual nanocrystals. Inset is a higher magnification image showing the near spherical morphology of the resulting nanocrystal, the scale bar is 100 nm. (b) Plot of the effective radius as a function of time for four individual nanocrystals. Inset are higher magnification images showing the faceted morphology of the resulting nanocrystals; the scale bars are 100 nm. (c) Logarithmic relationship between the effective radius and time. The red data points correspond to panel a, while the blue correspond to panel b, the different markers correspond to the individual nanocrystals indicated in the legends of panels a and b. The black lines are the average power law fits for the four different nanocrystals, obtained by linear regression. A 10 point averaging filter was used on data a−c to reduce noise in the data. Adapted with permission from ref 78. Copyright 2012 American Chemical Society.

of 0.58 to 0.71 nm which can be directly linked to the Ag_{13} cluster which has a size of 0.7 nm. However, also contained within this period were larger particles of about 10 nm which are considered to be a coalescence growth occurring at the same instance as the nucleation phase suggesting that the Ag_{13} clusters are created and consumed within this period. At 0.98 ms the average particle size was found to have increased from 0.71 to 3.36 nm suggesting that the Ag_{13} had been all used up in the formation of the higher particle size, however, growth through the addition of silver metal to the particles was ruled out as the next size particle which could be measured would have been Ag_{55} with a size of 1.2 nm but this was not seen within this synthesis. From 0.98 to 3.93 ms the particle size increased from 3.36 to 6.95 nm with a particle size of 20 nm found at 5.89 ms, however above 5.89 ms there was little to no change in particle diameter. Although, there was no change within particle size and the sharpening of the size distribution of the particles suggesting a rearrangement of transient aggregates. This synthesis can be divided in three stages which have been monitored through SAXS; first there is reduction of silver ions to silver metal; then the silver form Ag_{13} clusters as the dominant growth and finally these coalesce to form larger particles.

Perhaps the most useful technique for understanding the growth of silver nanoparticles within solution is in situ liquid cell TEM. Woehl et al.[78] have carried out the reduction of 1 mM aqueous silver nitrate through irradiation of electron beam within the TEM. When water is irradiated with an electron beam, it breaks down into numerous products such as e_{aq}^-, H^+, and OH^-. The reduction of the silver occurs then through either hydrogen radical or free electrons within solution.[79] Additional aqueous electrons could have also been created through irradiation of the silicon nitrate window used within the liquid cell and could have transferred to the aqueous solution.[80] Conversely to this, the silver can be oxidized by the hydroxyl radicals.[81] To investigate the nucleation and growth of silver nanoparticles Woehl et al. carried out different magnifications, electron beam currents and pixel dwell times. The nucleation phase remains somewhat unknown due to the resolution limit within the TEM. It is expected that LaMer[9] type burst nucleation occurs due to the short time required for the particles to become detectable. Using this system it was possible to study the growth of silver under both diffusion and surface reaction controlled growth. At high beam currents there is an abundance of reducing agent which reduces the silver ions within solution leading to diffusion limited growth.

The rate of growth within a diffusion limited regime was found to be $r \propto t^{1/8}$, Figure 19c which is 3 times smaller than the expected $t^{1/3}$ predicted in the LSW model, and currently this is still an active area of research. Although, it is suggested that the LSW model may not fit in this case as many of the silver particles grew on the silicon nitrate screen rather than free within the solution.

Furthermore, the particle density was very high which could have led to a suppression of growth. Growth at lower beam current shows an effective growth rate of $r \propto t^{1/2}$,

Figure 19b, which is consistent with the LSW model and it was discovered that crystalline seeds formed were random hexagonal close packed in nature. An attempt was made to determine the morphology of the crystallite, Figure 19, insert with the 60° edge angle along with the bright field contrast suggesting a trigonal plate morphology whereas the 120° suggests an icosahedral morphology or pentagonal bipyramid.

Nishimura et al.[82] carried out a synthesis of silver nanoparticles while monitoring UV−vis, XAFS and XANES. Their synthetic method was to reduce silver nitrate with sodium acrylate in the presence of NaOH in water. It was found that there was a very gradual color change from clear to yellow of the solution while refluxing with it being very much dependent on the ratio of NaOH to silver nitrate. The reaction containing a high amount of NaOH, a ratio of 1:3.6 silver: NaOH were found to progress much at high rate of reaction, Figure 20, where the tracking of the reaction kinetics was made possible through UV−vis spectroscopy following the surface plasmon resonance of 405 nm.

This change in rate could be explained through the reactive species within the reaction where the reactive species key was Ag_2O which is produced within silver solution of pH > 10.5.[83] This was confirmed through XAFS and XANES, Figure 21.

From this data Nishimura et al. were able to conclude a three-step mechanism: first Ag_2O was formed in solution with the quantity being dependent upon the ratio of silver nitrate to NaOH, following this the Ag_2O redissolves within solution during heating creating Ag^+ ions, finally the Ag^+ is reduced and

dx.doi.org/10.1021/cr400544s | Chem. Rev. XXXX, XXX, XXX−XXX

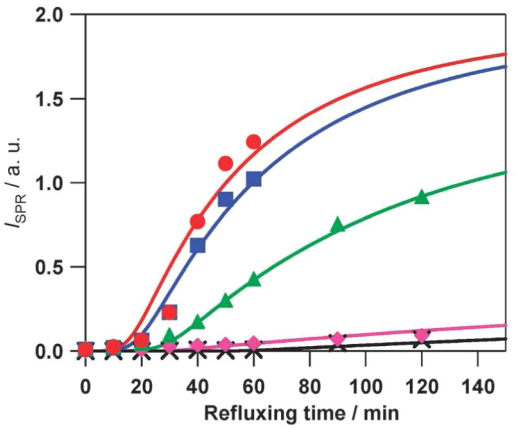

Figure 20. Time evolution of surface plasmon resonance intensity for the cases of x = 0 (×), 0.4 (diamond), 1.1 (triange), 1.8 (square), and 3.6 (circle) where x is the ratio of silver to NaOH, 1:x. Solid lines represent the calculation of results. Reproduced from ref 82 with permission of the PCCP Owner Societies.

nucleates within solution which is accelerated by increasing the NaOH concentration. Figure 22 shows a proposed mechanism including the case of $Ag(OH)_x$ which can occur with silver ions within a basic solution.[84,85]

A time-resolved in situ SAXS in conjunction with UV−vis and TEM was carried out by Polte et al.[86] on the formation of silver particles using sodium borohydride reducing silver perchlorate with and without the presence of PVP. Under this regime without any PVP present, it was found that within the first 100 ms particles of 1 nm rapidly form and following this after 400 ms there is a rapid increase in the number of particles of this size. It is important to note that 1 nm is the resolution of SAXS used and therefore any information below this particle's size was not measured. Within the next 2 s, the particles size steadily increased up to 4.6 nm with a decrease of the particles number.

This is indicative of a coalescent growth mechanism where smaller particles are coming together to produce larger particles reducing the total number of particles within solution. Similar effects are shown within the sample containing PVP. However, in this case the particles of around 1 nm were stabilized for up to 80 min before coalescence occurred. For both of these systems the method of formation is schematically shown in Figure 23.

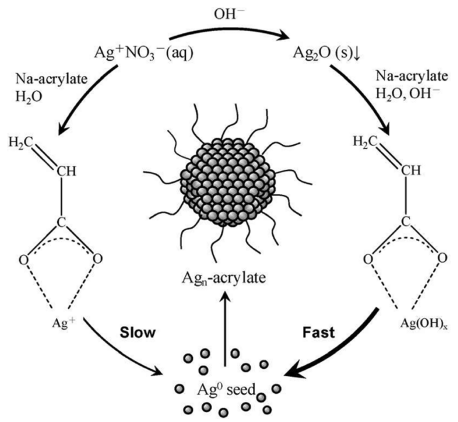

Figure 22. Mechanism for the formation of silver nanoparticles. Reproduced from ref 82 with permission of the PCCP Owner Societies.

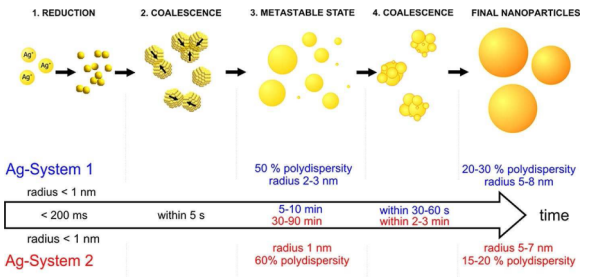

Figure 23. Schematic illustration of the deduced four-step growth mechanism of both silver nanoparticle systems. Reprinted with permission from ref 86. Copyright 2012 American Chemical Society.

4.3. Copper

The formation of copper nanoparticles was studied under UV−vis spectroscopy and time-resolved X-ray absorption near edge structure, TRXNES.[87] The reaction was carried out using copper acetylacetonate, $Cu(OAc)_2$ using $NaBH_4$ in the presence of poly(*N*-vinyl-2-pyrrolidone), PVP and NaOH to make the solution basic. The method of production is where $Cu(OAc)_2$ and PVP were mixed in water and then $NaBH_4$ and NaOH were injected under a nitrogen atmosphere at room temperature. The data obtained from the UV−vis spectroscopy showed that without PVP particles were unstable within solution and agglomerated with time, Figure 24.

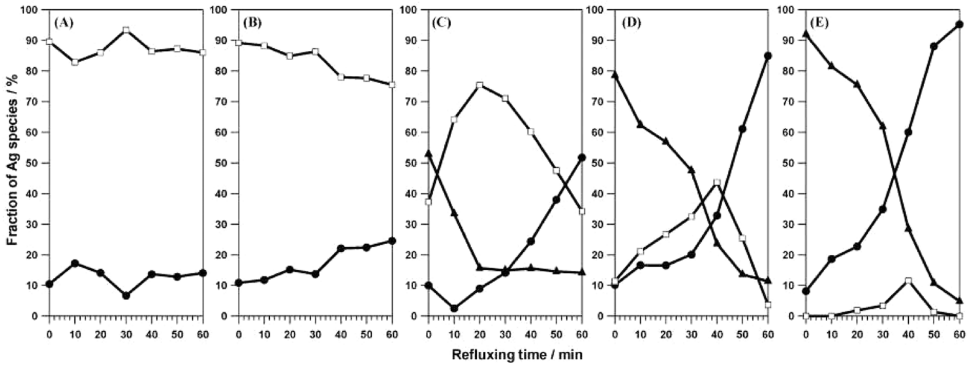

Figure 21. Time evolution of the fractions of each Ag species (ϕ_i) in the case of x = (A) 0, (B) 0.4, (C) 1.1, (D) 1.8, and (E) 3.6. Open square, circles and filled triangles correspond to ϕ_1[Ag^+ ($AgNO_3$)] ϕ_2 (Ag metal), and ϕ_3 [Ag^+ (Ag_2O origin)], respectively. Reproduced from ref 82 with permission of the PCCP Owner Societies.

dx.doi.org/10.1021/cr400544s | *Chem. Rev.* XXXX, XXX, XXX−XXX

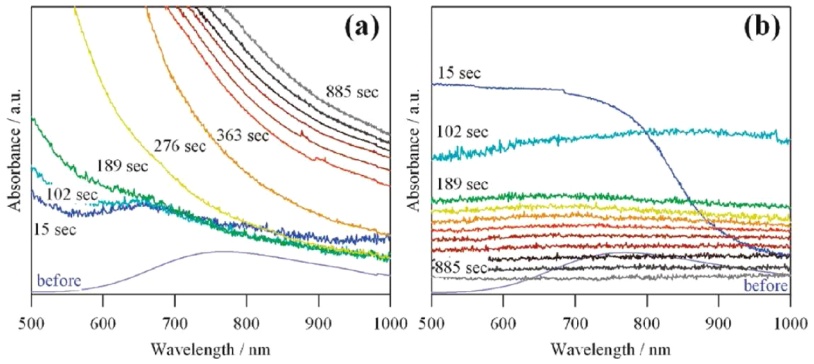

Figure 24. UV−vis spectra of reaction solution taken periodically in the (a) presence and (b) absence of PVP after injection of the $NaBH_4$/NaOH solution. Reprinted with permission from ref 87. Copyright 2009 American Chemical Society.

With the presence of PVP being as a key that a mechanism was formulated which was understood through TRXNES, Figure 25, where $Cu(OAc)_2$ forms copper hydroxide which

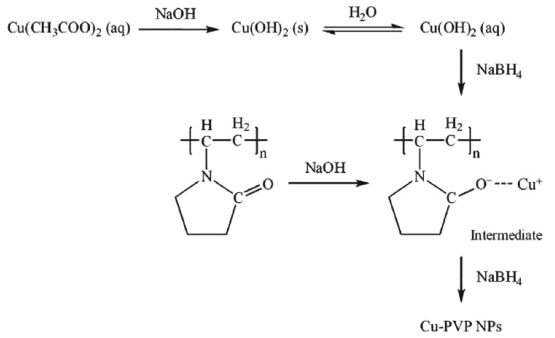

Figure 25. Formation mechanism of Cu nanoparticles. Reprinted with permission from ref 87. Copyright 2009 American Chemical Society.

then dissolves within the solution. The $NaBH_4$ then reduces the copper allowing it to bind to PVP through a Coulomb interaction which then in turn is reduced by $NaBH_4$ to form Cu nanoparticles.

In summary for this section, the gold nanoparticles can be divided into three different syntheses. The first is the reduction of $HAuCl_4$ using trisodium citrate in water, the second is the reduction of $HAuCl_4$ using sodium borohydride and finally the reduction of $HAuCl_4$ in the presence of citric acid and PVP. The most commonly studied is Turkevitch method for reducing the gold salt with trisodium citrate. This synthesis was originally thought to follow the LaMer type burst nucleation followed by Ostwald ripening which is true for near neutral pH values. However, it was discovered that at low pH values there was coalescence as the dominant form of growth before Ostwald ripening occurs. With the use of SAXS it was found that this coalescence also occurs within about 200 ms and followed by Ostwald ripening to form monodispersed particles.

Furthermore, drying the reaction and measuring the sample with an AFM led to channels between particles being detected showing explicitly the interparticle ripening which occurs. Within classical theory, all the reduction occurs at the start of the reaction in a burst formation. However, using XANES it was found that the reduction simultaneously occurs with the growth which was previously unseen.

The formation mechanism reducing using $NaBH_4$ (sodium borohydride) with no stabilizing surfactant was found to be a very fast formation of small nuclei followed by coalescence and then Ostwald ripening; this step of coalescence was not detected previously.

Finally, with PVP, $HAuCl_4$, and $NaBH_4$, it was found that coalescence also occurs with very small particle sizes. Additionally, within this case due to the stabilizing effect of the PVP, it was possible to isolate gold dimers, trimers, and Au_{13} nuclei. However, it is important to note that the initial growth occurs through a coalescent process followed by Ostwald ripening.

Importantly, within the formation of gold nanoparticles only one experiment carried out by Yao[45] was able to detect any portion of the nucleation mechanism. This is of the utmost importance as all other experiments trying to obtain information about the nucleation and growth of gold only delivers results within the growth regime.

The synthesis of silver nanoparticles has been carried out over numerous methods leading to different nucleation and growth regimes. From a LaMer burst nucleation followed by Ostwald ripening with a clearly separated growth phase to a mixed regime of nucleation and growth happening simultaneously. Additionally, there were numerous methods of growth occurring including autocatalytic surface reactions, coalescence and Ostwald ripening.

The growth of silver nanoparticles was well explored within all the literature reviewed, however, the nucleation method is lacking. Only within the work by Takesue,[77] they were able to detect through SAXS an Ag_{13} cluster showing the initial stages of silver particle formation which has eluded other researchers due to analytical technique resolution problems.

With both gold and silver a large knowledge gap within the nucleation of these materials. With the improvement of analytical techniques, one day it will be possible to probe materials on the atomic scale without disruption to the synthetic mechanism. With future advancement, it will be possible to fully analyze the formation of materials within the key step of nucleation.

5. METAL OXIDES

Iron ions in solution often form a hexahydrated ion which depends on the oxidation state and pH can undergo a hydroxylation reaction. For Fe(II) at room temperature the hydroxylation occurs at pH 7−9 where for Fe(III) the hydroxylation occurs from pH 1 to 4−5.[88,89] These metal hydroxylated complexes are unstable in solution and condense through two basic mechanisms depending upon the coordination shell of the iron ions. For both cases substitution occurs

dx.doi.org/10.1021/cr400544s | Chem. Rev. XXXX, XXX, XXX−XXX

through the nucleophilic character of hydroxo ligand. For $[M(OH)_h(OH_2)_{6-h}]^{(z-h)+}$, the condensation mechanism eliminates water to form hydroxo bridges, an olation mechanism, Figure 26.

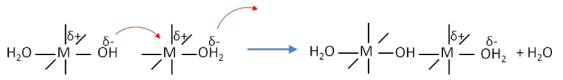

Figure 26. Olation mechanism for the condensation reaction where water is eliminated to form hydroxo bridges.

The rate of this reaction is very high due to the lability of the coordinated water molecules. For oxohydroxo complexes, $[MO_a(OH)_b]^{(z-2a-b)+}$, there is no coordinated waters which can be eliminated and so the condensation occurs through a two step associative process, Figure 27, leading to the formation of water and an oxo bridge, the oxolation mechanism.

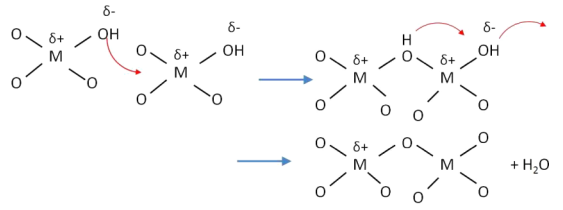

Figure 27. Formation of oxo bridges through a two step associative mechanism forming water.

The synthesis of metal oxides in a non aqueous environment occurs through the formation of an aldehyde radical. The formation of iron oxide from the decomposition of Fe(III) decanoate, Figure 28, occurs through a radical which forms from a reaction between the carboxylate and the iron leading to an oxygen on the iron which, in turn can then form an oxo bridge between irons.

If, however, the starting material does not have a similar carboxylic group such as Fe(acetylacetonate)$_3$ then ligand exchange occurs within solution to form an iron carboxylate first then to carry on with the scheme in Figure 28.[90]

Thermal decomposition is the most prevalent synthesis in nonaqueous media which has been followed using UV−vis spectroscopy which has shown promise when traceable materials are chosen as starting materials. One such case is work by Casula et al.[92] where iron oxide, Fe_3O_4, was synthesized through oxidizing $Fe(CO)_5$ with meta-chloroperoxybenzoic acid (mCPBA) in the presence of tridecanoic acid in dioctyl ether. The particles were formed using a hot injection method where $Fe(CO)_5$ and mCPBA were injected in a hot solution of tridecanoic acid at 293 °C. The oxidation reaction takes 1 h and there is no measurable formation of particles before 1 h.[93,94] A wavelength of 440 nm was chosen to track the reaction with time, Figure 29, allowing the reaction's nucleation

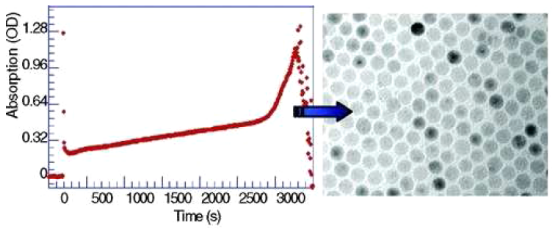

Figure 29. UV−vis spectra for the oxidation of $Fe(CO)_5$ by mCPBA showing burst nucleation. Reprinted with permission from ref 92. Copyright 2006 American Chemical Society.

to be followed. It was seen that the reaction undergoes bust nucleation following LaMer nucleation.[9,10] However, the nucleation is delayed. It is suggested that the time taken for the particle formation to occur is due to the low stability of the nuclei which leads to a very slow nucleation step. Following this slow nucleation there is an extremely fast growth which occurs at the 1 h mark.

To follow the nucleation and growth of iron oxide further studies were carried out by Kwon et al.,[26] where size exclusion chromatography, SEC, was carried out on aliquots taken from the reaction vessel. The synthetic method was the injection of iron-oleate into 1-octadecene at 120 °C and heating the mixture to 320 °C and holding the mixture at this temperature. By looking at a wavelength of 400 nm it was possible to detect both iron oxide nanocrystals and the iron-oleate complex. Figure 30 shows that there is two regions of retention, region (I) from 6.5 to 9 min and region (II) from 3 to 5.5 min. With time the peak in region I decreases whereas the peak in region (II) increasing, this is indicative of region (I) containing the peak for the starting material iron-oleate and any intermediate species.

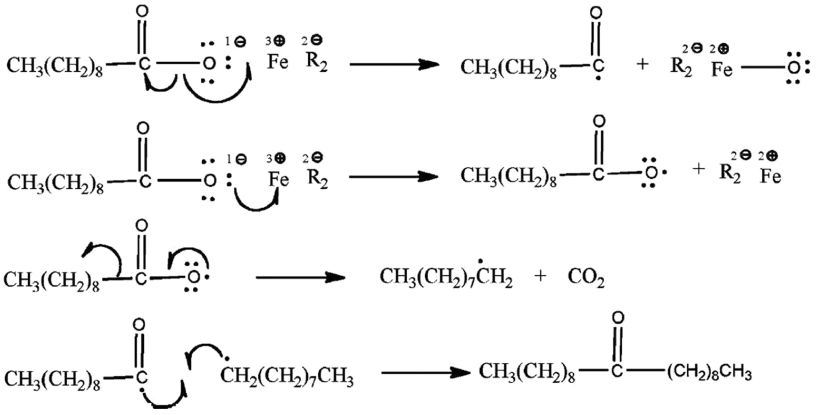

Figure 28. Example schematic for the formation of iron oxide through a radical in nonaqueous solutions. Reproduced from ref 91 with permission of the PCCP Owner Societies.

dx.doi.org/10.1021/cr400544s | Chem. Rev. XXXX, XXX, XXX−XXX

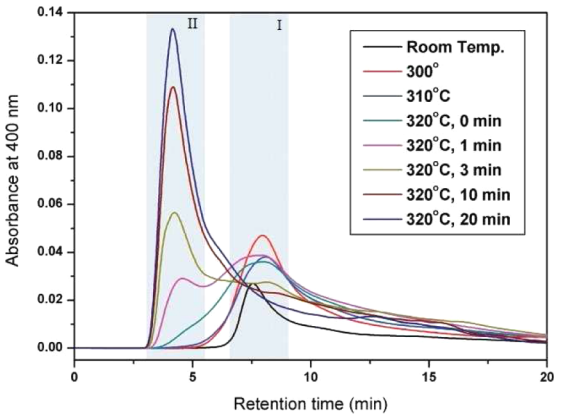

Figure 30. Chromatogram of absorbance at 400 nm of the sample aliquots drawn from the solution during the reaction for the synthesis of iron oxide nanocrystals. 1-Octadecene was used as a solvent for the reaction. Shaded areas indicate region I (right) and region II (left), respectively. Reprinted with permission from ref 26. Copyright 2007 American Chemical Society.

To further study this process electrochemical impedance spectroscopy was carried out to measure the uptake of Fe^{2+} and Fe^{3+} into iron oxide nanocrystals due to the low mobility of the nanocrystals being much lower than ionic species within solution. Therefore, it is estimated that the crystal yield can be measured from the change of impedance with time. Figure 31 shows the data agrees with the SEC data where iron-oleate and intermediates are quickly formed into nanocrystals. Particles were also studied under the TEM, and it was found that with time there was size focusing of the nanoparticle which is indicative of Ostwald ripening.

The method of nucleation is perhaps best understood for the metal oxides where the formation of the metal oxide bridges occurs through either hydroxylation or oxolation[88,89] additionally the synthesis within organic solution has been found to proceed through a free radical.[91] Although the pathways for which the particles nucleate and growth is already known there has been very little study of these processes most likely due to the lack of measurement techniques in the past. UV−visible spectroscopy has been widely used for both noble metals and quantum dots, but this is not a usable technique for metal oxides directly where there is no surface plasmon resonance, SPR. Casula et al.[92] overcame this lack of SPR indirectly through using mCPBA which does have a UV−vis peak which can be followed with time. The lack of SPR has led to the use of SEC and electrochemical impedance as methods of measuring the particle size with time.[26] Ideally metal oxide systems should be studied under similar techniques to that of the noble metals using SAXS in conjunction with XAFS or TRXNES to be able to measure both large and small size particles. This is an area that should be undergoing active research due to the current and future applications of these particles in biomedicine and other areas. Being able to understand these processes would allow for the synthesis to be much more reproducible than they are currently.

6. QUANTUM DOTS

The synthesis of semiconductor nanoparticles, quantum dots, has been studied using UV−vis spectroscopy to follow the evolution of nanoparticle growth within solution. Nuclear magnetic resonance (NMR)[95] and SAXS[96,97] were used to

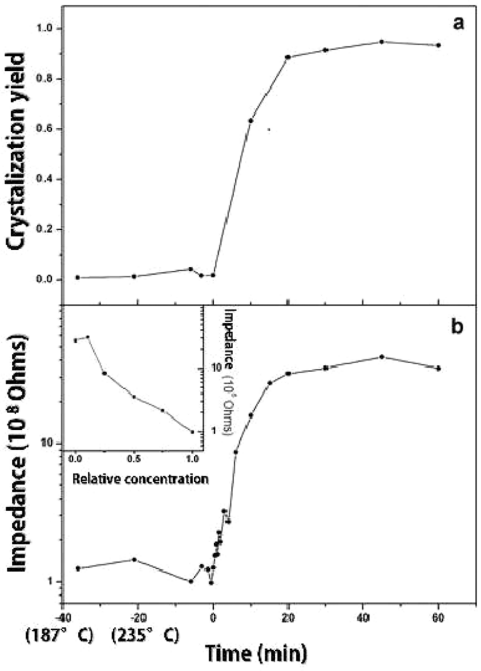

Figure 31. (a) Temporal change of the crystallization yield in the solution during the heating procedure measured by the elemental analysis. (b) AC impedance plot of the sample aliquots dispersed in THF, which were drawn from the solution during the heating procedure. In the inset, the dependence of AC impedance value on the iron-oleate concentration in the sample aliquot is plotted. Relative concentration is the iron-oleate concentration in the sample aliquot normalized by that of the original reaction solution. In the time axis in panels a and b, $t = 0$ when the solution temperature just reached 320 °C. For $t < 0$, the corresponding solution temperature for each time is indicated in the parentheses. 1-Octadecene was used as the solvent for all. Reprinted with permission from ref 26. Copyright 2007 American Chemical Society.

study the reaction further. The synthesis of quantum dots has been carried out over many years and within recent years efforts have been made to understand how these particles nucleate and grow within solution. The most recent developments are shown within this review.

6.1. Magic Size Nanoparticles

Magic size nanoparticles are particles which are of a well-defined size such as $(CdSe)_{34}$.[98] These are of particular interest as they are particularly stable[99,100] and have unique nucleation and growth routes. It has been suggest by Yu et al. that magic size particle only undergo a nucleation step without any further growth[101] and by Kudera et al.,[102] who suggested that due to stability Ostwald ripening can not occur as the small particles do not redissolve to increase the size of larger particles.

A further understanding of the process of the formation of magic size nuclei can be seen in work by Kudera[102] where different families of magic size particles were observed within solution through UV−vis spectroscopy. The synthesis of the CdSe was carried out by mixing dodecylamine and nonanoic acid with cadmium oxide at 200 °C under an inert atmosphere. Following this the solution was cooled to 80 °C and a solution of selenium in trioctylphosphine was added to the flask which was held at 80 °C for the reaction. The peaks within the UV−vis spectra, 330 nm and 350−360 nm, do not gradually shift with time. Instead the peaks slowly loose intensity and the peaks at 431 and 447 nm gain intensity, Figure 32. This

dx.doi.org/10.1021/cr400544s | Chem. Rev. XXXX, XXX, XXX−XXX

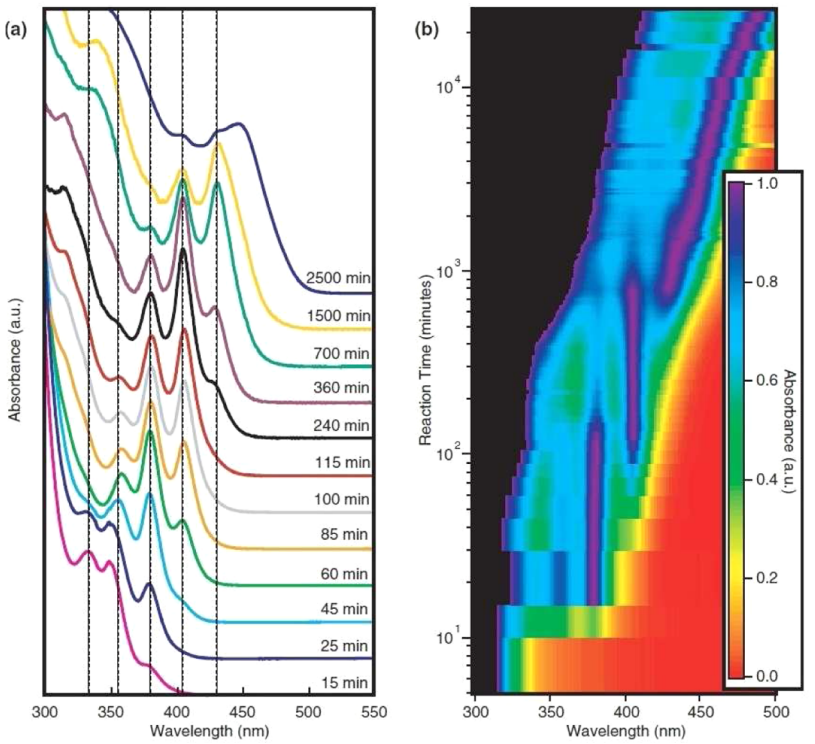

Figure 32. UV−vis absorption spectra of CdSe with time. Reprinted with permission from ref 102. Copyright 2007 WILEY-VCH Verlag GmbH & Co. KGaA, Weinheim.

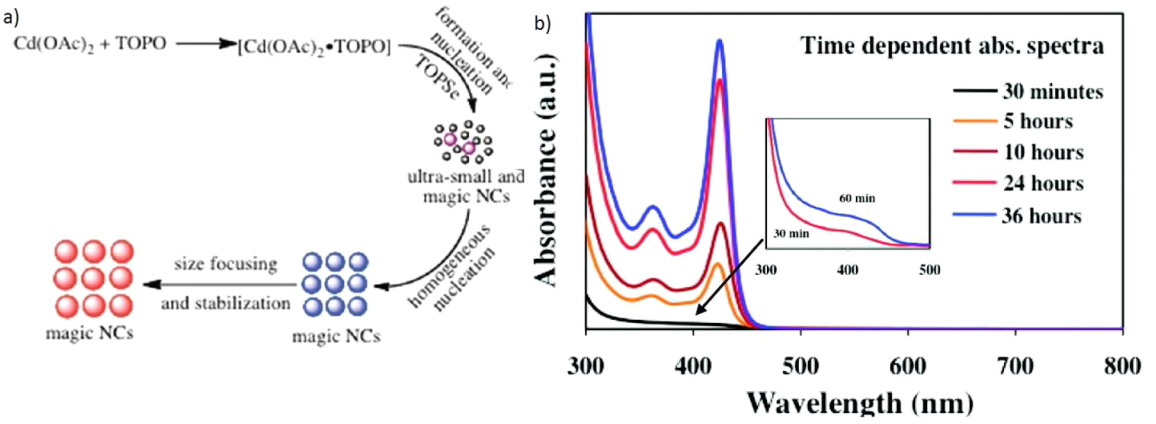

Figure 33. Reaction mechanism for the low temperature synthesis of CdSe capped with TOPO. Reprinted with permission from ref 103. Copyright 2012 American Chemical Society.

indicative of a system that is not undergoing Ostwald ripening as under this process the peak wavelengths would slowly red shift with time rather than loose intensity. Instead, the system is undergoing a series of growth steps where one family concentration increases with time while other diminish, tending toward larger family sizes.

Also the average size of a family does not appear to change time. This was further proven through using a Gaussian fit of the peaks using a model where the size of the particles can only increase with time, it was shown to have an excellent fit and further agreed upon by a control experiment. This control was carried out to determine if in the presence of no reactive monomers was there any Ostwald ripening or coalescence occurring. The synthesis was set up and left for many hours, following this an aliquot was extracted and thoroughly washed. The washed sample was then dissolved into a solution containing only surfactants and heated to 80 °C with the UV−vis spectra recorded over many hours. This showed no change with time agreeing with the model with that no Ostwald ripening or coalescence occurs.

Yu et al.[101] have suggested a thermodynamic explanation for the formation of magic size quantum dots by looking at the formation of the Cd and Se precursors within solution. The typical reaction conditions were $Cd(OAc)_2{\cdot}2H_2O$ and myristic acid were mixed in a flask with 1-octadecene and heated to 120 °C for 2 h. Selenium trioctylphosphine (SeTOP) was prepared through the sonication of Se powder in TOP at 60 °C.

Following this the two precurors were mixed at 100 °C and heated to 120 °C under a flow of nitrogen and following this heated to 240 or 150 °C and heated at this temperature for 40 or 60 min, respectively. The method of formation is thought to follow eqs 31−33. Equation 33 shows the formation of the

dx.doi.org/10.1021/cr400544s | *Chem. Rev.* XXXX, XXX, XXX−XXX

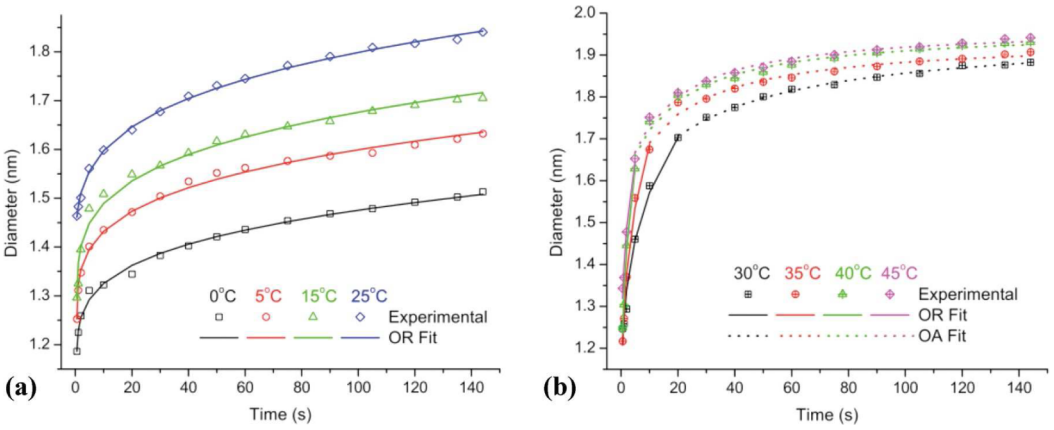

Figure 34. Variation in approximate average particle radius with time for thiolate-capped PbS nanocrystals grown by bottom-up reactions of Pb^{2+} and S^{2-} in water over the temperature range (a) 0−25 °C and (b) 30−45 °C. Symbols represent experimental measurements, while lines refer to calculated values for Ostwald Ripening (−) and orientated attachment (···) mechanisms. Reprinted with permission from ref 116. Copyright 2009 American Chemical Society.

magic size particles from solution; however, it is only valid when the chemical reaction kinetics are not a determining factor on the formation of magic-sized nuclei. Importantly with this equation it allows an understanding of the population and size of the $(CdSe)_m$(solid) where a balance between the effect of the synthetic parameters on the solubility/stability of $(CdSe)_m$(solid) and on the nucleation. The control of this fine balance comes from the rate of temperature increase where it needs to be slow enough to realize the thermodynamically driven (quantized nucleation) with no further growth. *P* corresponds to precursor.

$$(Cd)_P + (Se)_P \rightarrow (Cd - Se)(\text{soluble}) \quad (31)$$

$$(Cd - Se)(\text{soluble}) \rightleftharpoons (CdSe)_x(\text{soluble}) \quad (32)$$

$$(CdSe)_x(\text{soluble}) \rightleftharpoons (CdSe)_m(\text{solid}) \quad (33)$$

These equations were formulated through looking at the product of a series of reactions at different reaction temperatures looking at ^{31}P nuclear magnetic resonance.

It was discovered that there was a cross over between the formation of magic sized quantum dots to regular quantum dots which are highly dependent upon the temperature and choice of starting materials.

The concentration of the magic size nanoparticles was considered to be highly dependent upon the dissolution of $(CdSc)_m$(solid) which varied with temperature leading to the regular quantum dots at higher temperatures.

Work by Newton et al.[103] was carried out following the UV−vis spectra for the synthesis of CdSe using $Cd(acetate)_2$, $Cd(OAc)_2$ with selenium powder in the presence of trioctylphosphine oxide. The reaction mechanism is suggested in Figure 33a) where the formation of (reactive monomers) can be elucidated from the peak at 388 nm within the UV−vis spectra[95,104,105] along with a peak at 403 nm which is an indication of magic size nuclei of CdSe. Over 5 h of reaction time the solution red shifts to 422 nm which is indicative of the size focusing of particles and no further growth occurs due to the high stability of magic-sized particles.[99,100]

Although, following the UV−vis spectra does not directly measure the particle size within solution it is able to give an indication of the processes taking place and by measuring the full with half-maximum of the UV−vis peaks it was possible to estimate the size of the particles within solution which from the peak at 422 nm an estimation of the particle size is <2.0 nm in diameter.[99,100,106,107]

6.2. Regular Quantum Dots

Regular quantum dots have widely been studied with UV−vis spectroscopy.[108−115] Which is due to the formation of a set of empirical equations relating the size of these nanoparticles to their absorption spectra.[16−23]

The study of UV−vis spectroscopy which can elucidate the nucleation and growth of these quantum dots work by Brazeau et al.[116] has shown that there is a temperature dependence on the growth which occurs within PbS.

Figure 34 shows how the nanoparticle size changes with time for a series of reactions at different temperature. This data was then fitted to kinetic models for Ostwald ripening and orientated attachment.

It was found that at a low temperature, $0 \leq T \leq 25$ °C, for time, $t > 0.5$ s, Ostwald ripening dominated. Whereas at a high temperature, $30 \leq T \leq 45$ °C, growth dominated by Ostwald ripening at early times, $0 < t < 20$ s, and then orientated attachment. This can be rationalized through considering the energy of the system. At higher temperatures there will be larger thermal energy within the system which will increase Brownian motion. This increase in motion leads to a statistically more likely chance of the particles interacting at the correct crystallographic orientation for orientated attachment to occur.

To further understand the formation of ZnO, Caetano et al.[96] carried out with in situ XAFS, SAXS, and UV−vis spectroscopy.

The synthesis was carried out following the previously work by Spanhel and Anderson[117] where zinc acetate, Zn_4OAc_6, under went hydrolysis and condensation by potassium hydroxide, KOH, dissolved in absolute ethanol. There was found to be 4 stages of growth over a 1000 min reaction period; nucleation, growth of compact aggregates, growth of fractal aggregates and secondary nucleation and fractal aggregates growth.

The particle growth was found to be divided into 4 stages each with its own growth regime. The first stage $t < 5$ min it was found that the quantum dot radius increased from 1.8 to 2.1 nm though XAFS through a nucleation process. Stage 2−5

dx.doi.org/10.1021/cr400544s | *Chem. Rev.* XXXX, XXX, XXX−XXX

$< t <$ 100 min it was found that orientated attachment occurs through following SAXS data. To determine whether coalescence or orientated attachment occurred an orientated attachment model[118,119] was applied and was found to be an excellent match to the data. Within the third stage, $100 < t <$ 350 min was found to be due to cluster−cluster aggregation. Furthermore, due to the near linear growth of particle size fitting is in excellent agreement with theoretical and experimental data related to diffusion limited cluster−cluster aggregation.[120] The final stage $t > 350$ min the previous process of aggregation was disturbed through the secondary formation of ZnO. This secondary formation of ZnO leading to chemically unstable conditions is produced through the increase in water within the system which has been shown to have a noted effect on the ZnO production.[121−124] The formation of addition ZnO and along with changes to the slopes of SAXS data are consisted with cluster aggregation growth involving a polydisperse aggregation model.[120,125]

The four stages with resperct to the changes in size between both XAFS and SAXS are summarized in Figure 35 showing both the quantum dot radius from UV−vis and SAXS at each time period.

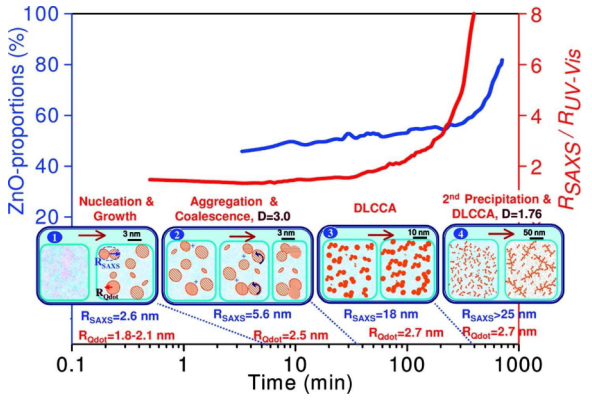

Figure 35. Schematic evolution of colloidal system as derived from the time evolution of the fractions of precursor and zinc oxide (XAFS), the quantum dot radius R_{UV-vis} and the aggregate of gyration radius R_g (SAXS). Reprinted with permission from ref 96. Copyright 2011 American Chemical Society.

The Stöber method[126] for the formation of silica nanoparticles has been studied over numerous years. The simple synthesis is used in the formation of silica nanoparticles and is the hydrolysis of tetraethyl orthosilicate, TEOS, using ammonia in ethanol.

Pontoni et al.[127] carried out SAXS experiments and discovered that the most likely growth mechanism is coalescence which is diffusion controlled after the initial nucleation phase.

Following this work, Green et al.[128] carried out a study of silica nanoparticles through DLS, dynamic light scattering, ^{29}Si NMR and SAXS all of which confirmed that through the Stöber method there was continuous nucleation in conjunction with controlled aggregation of primary particles.

In more recent time, a synthesis of silica nanoparticles showed peptides along with TEOS in ethanol a very slow change in supersaturation with time.[129−131]

A method was studied by Fouilloux et al.[132] using SAXS in which they discovered that LaMer mechanism and the classical nucleation theory did theoretically obtain both the correct size and particle concentration. It was unable to obtain the correct size distribution.

This was further studied using SAXS and Raman spectroscopy and it was discovered that most particles were created by coalescence, forming higher density particles with time.[97]

Figure 36a shows that the supersaturation does not reach a maximum until 100 min which is in conjunction with the scattering curves, Figure 36 (b), which have slopes less than expected for a dense homogeneous solid. As the consumption of Si with the solution occurs the gradient within the scattering curves increases which can be interpreted as an increase in density with time. Furthermore, at the maximum in supersaturation this corresponds to the time which particle volume would increase most rapidly; however, only a small change in particle radius is seen which is further indication of particle density increasing with time.

This restructuring which is not contained with in either classical nucleation theory nor kinetic nucleation theory[133] could lead to the highly monodispered nanoparticles which are the result of this synthesis, Figure 36 A and B.

In a recent research, the critical roles of cationic surfactants in the preparation of colloidal mesostructured silica nanoparticles has been explored by Yamada et al.[134] Moreover, De Paz-Simon et al.[135] have investigated a method to obtain periodic mesostructured silica films using UV light.

A recent review of the monomer effects on nucleation and growth for CdSe in 1-octadecene was carried out by Yu.[138] In brief, the formation of the nanoparticles either magic sized nuclei or regular quantum dots is very much dependent upon the formation of the monomers required to make the particle. The route of formation has been studied for very few systems such as Cd and Zn chalcogenide[104,136,137] and PbSe.[95] The mechanism is proposed to be where trialkylphosphine chalcogenides deoxygenate the oleic acid or phosphonic acid surfactant to generate trialkylphosphine oxide and oleic or phosphonic acid anhydride products, Figure 37.

Furthermore, within this review by Yu[138] the starting material was often cadmium (acetate)$_2$, Cd(OAc)$_2$, which can be either singly or doubly ligand exchanged with oleic acid to then go on and form a CdSe monomer. For the doubly exchanged it was possible to form the magic size nuclei for high level of supersaturation and regular nuclei for lower level of supersaturation. Whereas for the singly exchanged, Cd(OAc)-(oleate) complex, only the magic sized nuclei formed.

In general, the study of quantum dots has been led through UV−vis spectroscopy due to quantum confinement effects, however, these analyses largely depend upon empirical calculations to obtain particle sizes. To further study the formation processes, ^{31}P was used to show the initial stages of the reactive species formation but it has not given any further insight into particle formation. Within the field of magic sized quantum dots, UV−vis spectroscopy is ideal for measuring the particle size even with empirical calculations due to the discrete sizes of particle which occur with little size variance. However, the region between discrete sizes of magic sized quantum dots is ill-defined with a simple suggestion that particles are not stable between the two points and rapidly grow or redissolve to change size with no measurements of this area most likely due to the rate of reaction. This is a rather gray area where the information between these two points is unknown as analysis has not been fully explored. As there is no obvious peaks appearing within the UV−vis spectra perhaps XAFS could be ideal for this study if there is an unknown intermediate present

dx.doi.org/10.1021/cr400544s | Chem. Rev. XXXX, XXX, XXX−XXX

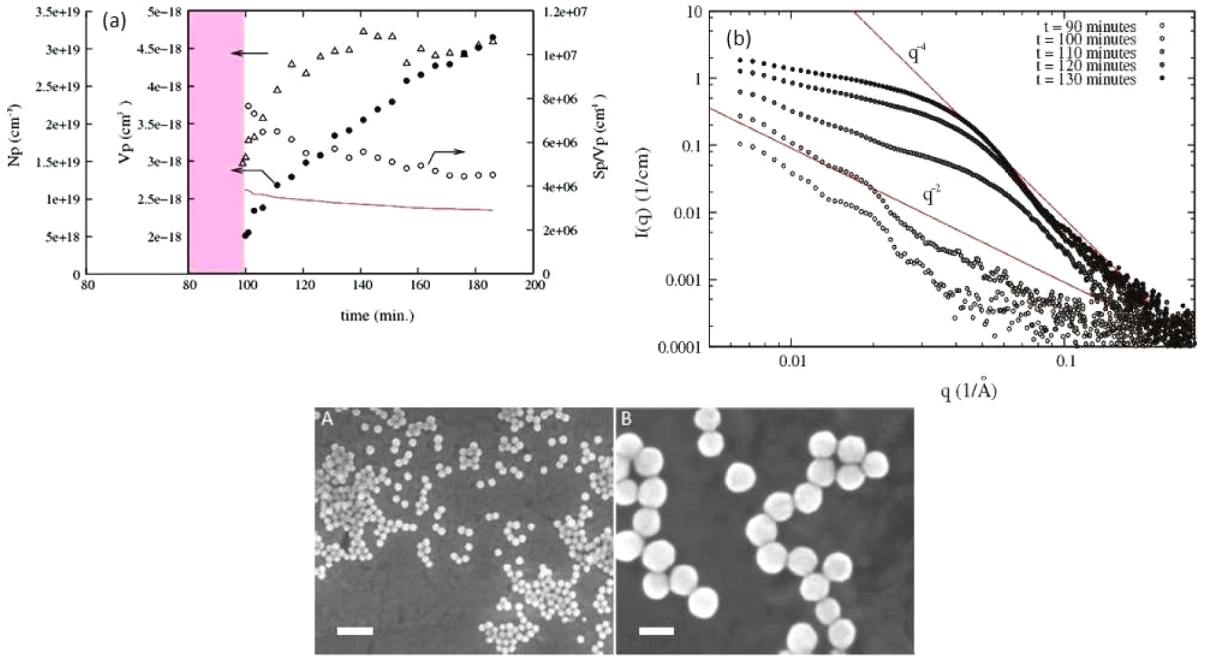

Figure 36. (a) Evolution of the scatterer's volume V_p(●), the particle number concentration (Δ with ρ assumed to be 2.2 g/cm^3), and the scatterer's surface to volume ration S_p/V_p(○) as a function of the reaction time for C = 40 mM and T = 80 °C. The line represents the surface volume ratio of a sphere of volume V_p. The gray box before t = 100 min indicates the absence of a defined Porod limit.(b) small-angle X-ray scattered intensity as a function of time for the sample prepared with 20 mM of L-arginine and T = 70 °C. Scanning electron microscope image obtained at the end of the reaction time($C_{L-arginine}$ = 6 mM, T = 65 °C). The scale bar is 200 nm for (A) and 40 nm for (B). Reprinted with permission from ref 97. Copyright 2011 American Chemical Society.

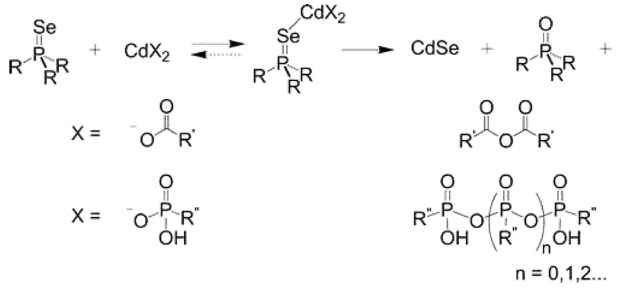

Figure 37. Formation mechanism for the monomer CdSe. Reprinted with permission from ref 136. Copyright 2007 American Chemical Society.

or even SAXS if the intermediate is lived long enough with an appropriate size.

Regular size quantum dotes have recently been studied using SAXS showing numerous growth techniques such as Ostwald ripening, coalescence, orientated attachment and diffusion limited cluster−cluster aggregative growth. Within all these experiments the nucleation phase of the particle is very much missing there is no understanding of how the nucleates form within solution then somehow combine to form a measurable species. This is somewhat understandable due to the resolution which SAXS or TEM provides and more research is required to really understand what is occurring with quantum dots nucleation and growth. Other classes of nanomateriales as zeolites, ordered mesoporous solids and metal organic framework are reviewed elsewhere.[135,139] Therefore, in this review only gold, silver, metal oxide nanoparticles, and semiconductor quantum dots are covered.

7. CONCLUSION, OUTLOOK, AND PERSPECTIVE

This review provides an overview of classical nucleation theory and growth starting at basic principals to obtain the formation of how particles form within solution. This theory gives a basic outline of how to control particle formation within solution by elucidating the key controllable parameters: reaction temperature, supersaturation, time and the surface energy which can be controlled indirectly through the choice of surfactants. Following this, a basic description of the different nucleation and growth mechanisms can occur within solution such as LaMer nucleation, Finke-Watzky two step mechanism, Ostwald ripening, digestive ripening, coalescence and orientated attachment, and intraparticle growth.

The mechanism of nucleation and growth of all nanoparticle is an area of intense interest as it will grant control over the nanoparticles synthesis including particle size and monodispersity. The limits within this field are the present analytical techniques: previously ex situ analysis was the only option to determine any information about the nucleation and growth mechanism. Although, it is important not to discount a simple method, there is a movement toward high resolutions in situ measurements of particle size and distribution through TEM and SAXS. This allows the gathering of information directly from the reaction mixture without having to worry about potential changes which might occur due to either sampling process disturbing the reaction mixture or changes occurring between the sampling point and analysis. The limitations of any analytical technique in this field is the resolution as there is still a missing link between free atoms in solution and small nuclei. There is limited information which can be gathered by XAFS, which with theoretical modeling can lead to the identification of small nuclei indirectly within solution.

dx.doi.org/10.1021/cr400544s | Chem. Rev. XXXX, XXX, XXX−XXX

As seen, within this review each material will nucleate and grow depending on its reaction conditions and even a small change in condition, such as pH, can lead to a completely different mechanisms. This leads to the question about the possibility to predict the nanoparticle formation mechanisms. Currently the authors believe that not yet, the prediction can not be made as a small change in reaction conditions can lead to unforeseen changes within the reaction mixture such as the formation of a metastable reactant. However, further analysis of these mechanisms will open the possibility to predict how a particle will form within solution and therefore obtain control of the synthesis much faster compared to the current methods of trial and error to optimize syntheses. The future within this research area is similar to a game of pass the parcel where, as analytical techniques improve, a new layer of wrapping paper can be removed until the present inside is found, so then a fully understood mechanism of particle nucleation and growth.

AUTHOR INFORMATION

Corresponding Author

*E-mail: ntk.thanh@ucl.ac.uk.

Notes

The authors declare no competing financial interest.

Biographies

Professor Nguyen T. K. Thanh FRSC MInstP is Professor of Nanomaterials at University College London, U.K. (http://www.ntkthanh.co.uk). She has over 13 years of research experience in synthesis and biofunctionalisation of inorganic nanoparticles for biomedical applications. She has been an invited speaker at over 100 international conferences and research departments and institutions all over the world. She has served on organisation and scientific committees for many major international conferences on Nanoparticles research (e.g., Scientific Chair of Faraday Discussion 175: "Physical Chemistry of Functionalised Biomedical Nanoparticle" in 2014 in UK, http://rsc.li/fd175; and organizer of Biohybrid NanoMaterials – Design and Applications Symposium, ICMAT, Singapore, June 2015, http://www.mrs.org.sg/. She was the Guest Editor of *Philosophical Transactions of the Royal Society A* on "Nanoparticles" theme issue published in September 2010. Recently she edited a seminal book: "Magnetic nanoparticles: From fabrication to clinical applications" published by CRC Press/Taylor and Francis in 2012. She was also the Guest Editor of *Nanoscale* themed issue "Functional nanoparticles for biomedical applications" published in 2013.

Niall M. Maclean obtained his MSci from the University of Glasgow in 2011. Following this he undertook a MRes in Molecular Modelling and Materials Science at University College London which lead into a Ph.D. under the supervision of Professor Nguyen T. K. Thanh based at UCL Healthcare Biomagnetic and Nanomaterials Laboratories. His interests are within the synthesis of magnetic nanoparticles for biomedical applications.

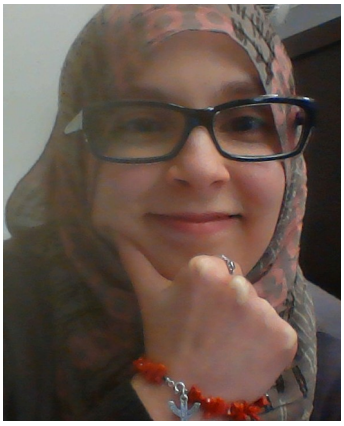

Sara Mahiddine obtained her Masters degree in condensed matter and nanophysics from Université Louis Pasteur Strasbourg and Institut de physique et chimie des matériaux Strasbourg, France in 2012. Currently she is studying materials and nanoscience at Université Louis Pasteur Strasbourg France and doing an internship under supervision of Professor Nguyen T. K. Thanh based at UCL Healthcare Biomagnetic and Nanomaterials Laboratories. Her interests are synthesis, characterization of superparamagnetic nanoparticles and the study of their different properties for biomedical applications.

ACKNOWLEDGMENTS

N.T.K.T. thanks the Royale Society for her Royal Society University Research Fellowship.

REFERENCES

(1) Thanh, N. T. K. *Magnetic Nanoparticles: from Fabrication to Clinical Applications*; CRC Press/Taylor and Francis: Boca Raton, FL/London, 2012.
(2) Pankhurst, Q. A.; Thanh, N. T. K.; Jones, S. K.; Dobson, J. *J. Phys. D: App. Phys.* **2009**, *42*, 224001.
(3) Narayanan, R.; El-Sayed, M. A. *J. Phys. Chem. B* **2005**, *109*, 12663.
(4) Astruc, D.; Lu, F.; Aranzaes, J. R. *Angew. Chem., Int. Ed.* **2005**, *44*, 7852.
(5) Bönnemann, H.; Richards, R. *Eur. J. Inorg. Chem.* **2001**, *2001*, 2455.
(6) Hyeon, T. *Chem. Commun.* **2003**, 927.
(7) Sozer, N.; Kokini, J. L. *Trends Biotechnol.* **2009**, *27*, 82.

(8) Atwater, H. A.; Polman, A. *Nat. Mater.* **2010**, *9*, 205.
(9) LaMer, V. K.; Dinegar, R. H. *J. Am. Chem. Soc.* **1950**, *72*, 4847.
(10) LaMer, V. K. *Ind. Eng. Chem.* **1952**, *44*, 1270.
(11) Ostwald, W. *Z. Phys. Chem.* **1900**, *34*, 495.
(12) Reiss, H. *J. Chem. Phys.* **1951**, *19*, 482.
(13) Lifshitz, I.; Slyozov, V. *J. Phys. Chem. Solids.* **1961**, *19*, 35.
(14) Wagner, C. *Ber. Bunsen-Ges. Phys. Chem.* **1961**, *65*, 581.
(15) Watzky, M. A.; Finke, R. G. *Chem. Mater.* **1997**, *9*, 3083.
(16) Yu, W. W.; Qu, L.; Guo, W.; Peng, X. *Chem. Mater.* **2003**, *15*, 2854.
(17) Mikulec, F. V.; Kuno, M.; Bennati, M.; Hall, D. A.; Griffin, R. G.; Bawendi, M. G. *J. Am. Chem. Soc.* **2000**, *122*, 2532.
(18) Rogach, A. L.; Eychmuller, A.; Hickey, S. G. *Small* **2007**, *3*, 537.
(19) Schmelz, O.; Mews, A.; Basché, T. T.; Herrmann, A.; Müllen, K. *Langmuir* **2001**, *17*, 2861.
(20) Cademartiri, L.; Montanari, E.; Calestani, G.; Migliori, A.; Guagliardi, A.; Ozin, G. A. *J. Am. Chem. Soc.* **2006**, *128*, 10337.
(21) Sun, J.; Goldys, E. M. *J. Phys. Chem. C* **2008**, *112*, 9261.
(22) van Embden, J.; Jasieniak, J.; Mulvaney, P. *J. Am. Chem. Soc.* **2009**, *131*, 14299.
(23) Jasieniak, J.; Smith, L.; Embden, J. v.; Mulvaney, P.; Califano, M. *J. Phys. Chem. C* **2009**, *113*, 19468.
(24) Zheng, H.; Smith, R. K.; Jun, Y.-w.; Kisielowski, C.; Dahmen, U.; Alivisatos, A. P. *Science.* **2009**, *324*, 1309.
(25) Kwon, S. G.; Hyeon, T. *Small.* **2011**, *7*, 2685.
(26) Kwon, S. G.; Piao, Y.; Park, J.; Angappane, S.; Jo, Y.; Hwang, N.-M.; Park, J.-G.; Hyeon, T. *J. Am. Chem. Soc.* **2007**, *129*, 12571.
(27) Finney, E. E.; Finke, R. G. *J. Colloid Interface Sci.* **2008**, *317*, 351.
(28) Zhang, R.; Khalizov, A.; Wang, L.; Hu, M.; Xu, W. *Chem. Rev.* **2012**, *112*, 1957.
(29) Carbone, L.; Cozzoli, P. D. *Nano Today* **2010**, *5*, 449.
(30) Mullin, J. W. *In Crystallization*; Mullin, J. W., Ed.; Butterworth-Heinemann: Boston, 1997.
(31) Puntes, V. F.; Zanchet, D.; Erdonmez, C. K.; Alivisatos, A. P. *J. Am. Chem. Soc.* **2002**, *124* (43), 12874.
(32) Robinson, I.; Zacchini, S.; Tung, L. D.; Maenosono, S.; Thanh, N. T. K. *Chem. Mater.* **2009**, *21* (13), 3021.
(33) Habraken, W. J. E. M.; Tao, J.; Brylka, L. J.; Friedrich, H.; Bertinetti, L.; Schenk, A. S.; Verch, A.; Dmitrovic, V.; Bomans, P. H. H.; Frederik, P. M.; Laven, J.; van der Schoot, P.; Aichmayer, B.; de With, G.; DeYoreo, J. J.; Sommerdijk, N. A. J. M. *Nat. Commun.* **2013**, *4*, 1507.
(34) Volmer, M.; Weber, A. *Phys. Chem.* **1926**, *119*, 277.
(35) Sugimoto, T. *Monodispersed Particles*; Elsevier: Amsterdam, 2001.
(36) Rao, C. N. R.; ; Achim Müller and Cheetham, A. K. *Nanomaterials Chemistry: recent developments and new directions*; Wiley-VCH Verlag GmbH Co. KGaA: Weinheim, Germany, 2007; p 139.
(37) Talapin, D. V.; Rogach, A. L.; Haase, M.; Weller, H. *J. Phys. Chem. B* **2001**, *105*, 12278.
(38) Rogach, A.; Talapin, D.; Shevchenko, E.; Kornowski, A.; Haase, M.; Weller, H. *Adv. Funct. Mater.* **2002**, *12*, 653.
(39) Sugimoto, T.; Shiba, F.; Sekiguchi, T.; Itoh, H. *Colloids Surf., A* **2000**, *164*, 183.
(40) Sugimoto, T.; Shiba, F. *Colloids Surf., A* **2000**, *164*, 205.
(41) Sugimoto, T. *J. Colloid Interface Sci.* **2007**, *309*, 106.
(42) Lee, W.-r.; Kim, M. G.; Choi, J.-r.; Park, J.-I.; Ko, S. J.; Oh, S. J.; Cheon, J. *J. Am. Chem. Soc.* **2005**, *127*, 16090.
(43) Watzky, M. A.; Finney, E. E.; Finke, R. G. *J. Am. Chem. Soc.* **2008**, *130*, 11959.
(44) Besson, C.; Finney, E. E.; Finke, R. G. *J. Am. Chem. Soc.* **2005**, *127*, 8179.
(45) Yao, S.; Yuan, Y.; Xiao, C.; Li, W.; Kou, Y.; Dyson, P. J.; Yan, N.; Asakura, H.; Teramura, K.; Tanaka, T. *J. Phys. Chem. C* **2012**, *116*, 15076.
(46) Niederberger, M.; Colfen, H. *Phys. Chem. Chem. Phys.* **2006**, *8*, 3271.
(47) Li, D.; Nielsen, M. H.; Lee, J. R. I.; Frandsen, C.; Banfield, J. F.; De Yoreo, J. J. *Science* **2012**, *336*, 1014.
(48) Penn, R.; Banfield, J. F. *Geochim. Cosmochim. Acta* **1999**, *63*, 1549.
(49) Peng, X.; Manna, L.; Yang, W.; Wickham, J.; Scher, E.; Kadavanich, A.; Alivisatos, A. P. *Nature* **2000**, *404*, 59.
(50) Peng, Z. A.; Peng, X. *J. Am. Chem. Soc.* **2001**, *123*, 1389.
(51) Faraday, M. *Philos. Trans. R. Soc. London* **1857**, *147*, 145−181.
(52) Turkevich, J.; Stevenson, P. C.; Hillier, J. *Discuss. Faraday Soc.* **1951**, *11*, 55.
(53) Wang, J.; Boelens, H. F. M.; Thathagar, M. B.; Rothenberg, G. *ChemPhysChem* **2004**, *5*, 93.
(54) Abécassis, B.; Testard, F.; Spalla, O.; Barboux, P. *Nano Lett.* **2007**, *7*, 1723.
(55) Abécassis, B.; Testard, F.; Kong, Q.; Francois, B.; Spalla, O. *Langmuir* **2010**, *26*, 13847.
(56) Ji, X.; Song, X.; Li, J.; Bai, Y.; Yang, W.; Peng, X. *J. Am. Chem. Soc.* **2007**, *129*, 13939.
(57) Chow, M.; Zukoski, C. *J. Colloid Interface Sci.* **1994**, *165*, 97.
(58) Yao, T.; Sun, Z.; Li, Y.; Pan, Z.; Wei, H.; Xie, Y.; Nomura, M.; Niwa, Y.; Yan, W.; Wu, Z.; Jiang, Y.; Liu, Q.; Wei, S. *J. Am. Chem. Soc.* **2010**, *132*, 7696.
(59) Pong, B.-K.; Elim, H. I.; Chong, J.-X.; Ji, W.; Trout, B. L.; Lee, J.-Y. *J. Phys. Chem. C* **2007**, *111*, 6281.
(60) Polte, J.; Ahner, T. T.; Delissen, F.; Sokolov, S.; Emmerling, F.; Thunemann, A. F.; Kraehnert, R. *J. Am. Chem. Soc.* **2010**, *132*, 1296.
(61) Madras, G.; McCoy, B. J. *J. Chem. Phys.* **2002**, *117*, 8042.
(62) Mandal, M.; Ghosh, S. K.; Kundu, S.; Esumi, K.; Pal, T. *Langmuir* **2002**, *18*, 7792.
(63) Polte, J.; Erler, R.; Thunemann, A. F.; Sokolov, S.; Ahner, T. T.; Rademann, K.; Emmerling, F.; Kraehnert, R. *ACS Nano* **2010**, *4*, 1076.
(64) Polte, J.; Herder, M.; Erler, R.; Rolf, S.; Fischer, A.; Wurth, C.; Thunemann, A. F.; Kraehnert, R.; Emmerling, F. *Nanoscale* **2010**, *2*, 2463.
(65) Mikhlin, Y.; Karacharov, A.; Likhatski, M.; Podlipskaya, T.; Zubavichus, Y.; Veligzhanin, A.; Zaikovski, V. *J. Colloid Interface Sci.* **2011**, *362*, 330.
(66) Shields, S. P.; Richards, V. N.; Buhro, W. E. *Chem. Mater.* **2010**, *22*, 3212.
(67) Henglein, A.; Giersig, M. *J. Phys. Chem. B* **1999**, *103*, 9533.
(68) Harada, M.; Katagiri, E. *Langmuir* **2010**, *26*, 17896.
(69) Gubanov, P. Y.; Maksimov, I. L.; Morozov, V. P. *Mod. Phys. Lett. B* **2007**, *21*, 941.
(70) Lo, A.; Skodje, R. T. *J. Chem. Phys.* **2000**, *112*, 1966.
(71) Robson, J. D. *Mater. Sci. Technol.* **2004**, *20*, 441.
(72) Brown, L. *Acta Metall.* **1989**, *37*, 71.
(73) Coughlan, S.; Fortes, M. *Scr. Metall. Mater.* **1993**, *28*, 1471.
(74) Richards, V. N.; Rath, N. P.; Buhro, W. E. *Chem. Mater.* **2010**, *22*, 3556.
(75) Huang, F.; Zhang, H.; Banfield, J. F. *Nano Lett.* **2003**, *3*, 373.
(76) Hiramatsu, H.; Osterloh, F. E. *Chem. Mater.* **2004**, *16*, 2509.
(77) Takesue, M.; Tomura, T.; Yamada, M.; Hata, K.; Kuwamoto, S.; Yonezawa, T. *J. Am. Chem. Soc.* **2011**, *133*, 14164.
(78) Woehl, T. J.; Evans, J. E.; Arslan, I.; Ristenpart, W. D.; Browning, N. D. *ACS Nano* **2012**, *6*, 8599.
(79) Bogle, K. A.; Dhole, S. D.; Bhoraskar, V. N. *Nanotechnology* **2006**, *17*, 3204.
(80) Le Caer, S. *Water.* **2011**, *3*, 235.
(81) Belloni, J. *Catal. Today.* **2006**, *113*, 141.
(82) Nishimura, S.; Mott, D.; Takagaki, A.; Maenosono, S.; Ebitani, K. *Phys. Chem. Chem. Phys.* **2011**, *13*, 9335.
(83) Murray, B. J.; Li, Q.; Newberg, J. T.; Menke, E. J.; Hemminger, J. C.; Penner, R. M. *Nano Lett.* **2005**, *5*, 2319.
(84) Evanoff, D. D.; Chumanov, G. *J. Phys. Chem. B* **2004**, *108*, 13948.
(85) Biedermann, G.; Sillen, L. G. *Acta Chem. Scand.* **1960**, *14*, 717.
(86) Polte, J.; Tuaev, X.; Wuithschick, M.; Fischer, A.; Thuenemann, A. F.; Rademann, K.; Kraehnert, R.; Emmerling, F. *ACS Nano* **2012**, *6*, 5791.

(87) Nishimura, S.; Takagaki, A.; Maenosono, S.; Ebitani, K. *Langmuir* **2009**, *26*, 4473.
(88) Jolivet, J.-P.; Chaneac, C.; Tronc, E. *Chem. Commun.* **2004**, 477.
(89) Jolivet, J.-P.; Tronc, E.; Chan'eac, C. *C. R. Geosci.* **2006**, *338*, 488.
(90) Grabs, I.-M.; Bradtmöller, C.; Menzel, D.; Garnweitner, G. *Cryst. Growth Des.* **2012**, *12*, 1469.
(91) Perez, N.; Lopez-Calahorra, F.; Labarta, A.; Batlle, X. *Phys. Chem. Chem. Phys.* **2011**, *13*, 19485.
(92) Casula, M. F.; Jun, Y.-w.; Zaziski, D. J.; Chan, E. M.; Corrias, A.; Alivisatos, A. P. *J. Am. Chem. Soc.* **2006**, *128*, 1675.
(93) Bentzon, M. D.; van Wonterghem, J.; Mørup, S.; Thölén, A.; Koch, C. J. W. *Philos. Mag. B* **1989**, *60*, 169.
(94) Dante, S.; Hou, Z.; Risbud, S.; Stroeve, P. *Langmuir* **1999**, *15*, 2176.
(95) Steckel, J. S.; Yen, B. K. H.; Oertel, D. C.; Bawendi, M. G. *J. Am. Chem. Soc.* **2006**, *128*, 13032.
(96) Caetano, B. L.; Santilli, C. V.; Meneau, F.; Briois, V.; Pulcinelli, S. H. *J. Phys. Chem. C* **2011**, *115*, 4404.
(97) Fouilloux, S.; Tachë, O.; Spalla, O.; Thill, A. *Langmuir* **2011**, *27*, 12304.
(98) Bowers, M. J.; McBride, J. R.; Rosenthal, S. J. *J. Am. Chem. Soc.* **2005**, *127*, 15378.
(99) Park, Y.-S.; Dmytruk, A.; Dmitruk, I.; Kasuya, A.; Okamoto, Y.; Kaji, N.; Tokeshi, M.; Baba, Y. *J. Phys. Chem. C* **2010**, *114*, 18834.
(100) Kasuya, A.; Sivamohan, R.; Barnakov, Y. A.; Dmitruk, I. M.; Nirasawa, T.; Romanyuk, V. R.; Kumar, V.; Mamykin, S. V.; Tohji, K.; Jeyadevan, B.; Shinoda, K.; Kudo, T.; Terasaki, O.; Liu, Z.; Belosludov, R. V.; Sundararajan, V.; Kawazoe, Y. *Nat. Mater.* **2004**, *3*, 99.
(101) Yu, K.; Hu, M. Z.; Wang, R.; Piolet, M. L.; Frotey, M.; Zaman, M. B.; Wu, X.; Leek, D. M.; Tao, Y.; Wilkinson, D.; Li, C. *J. Phys. Chem. C* **2010**, *114*, 3329.
(102) Kudera, S.; Zanella, M.; Giannini, C.; Rizzo, A.; Li, Y.; Gigli, G.; Cingolani, R.; Ciccarella, G.; Spahl, W.; Parak, W.; Manna, L. *Adv. Mater.* **2007**, *19*, 548.
(103) Newton, J. C.; Ramasamy, K.; Mandal, M.; Joshi, G. K.; Kumbhar, A.; Sardar, R. *J. Phys. Chem. C* **2012**, *116*, 4380.
(104) Owen, J. S.; Chan, E. M.; Liu, H.; Alivisatos, A. P. *J. Am. Chem. Soc.* **2010**, *132*, 18206.
(105) Rempel, J. Y.; Bawendi, M. G.; Jensen, K. F. *J. Am. Chem. Soc.* **2009**, *131*, 4479.
(106) Park, Y.-S.; Dmytruk, A.; Dmitruk, I.; Kasuya, A.; Takeda, M.; Ohuchi, N.; Okamoto, Y.; Kaji, N.; Tokeshi, M.; Baba, Y. *ACS Nano* **2010**, *4*, 121.
(107) Cossairt, B. M.; Owen, J. S. *Chem. Mater.* **2011**, *23*, 3114.
(108) Xie, R.; Li, Z.; Peng, X. *J. Am. Chem. Soc.* **2009**, *131*, 15457.
(109) Rath, T.; Kunert, B.; Resel, R.; Fritz-Popovski, G.; Saf, R.; Trimmel, G. *Inorg. Chem.* **2008**, *47*, 3014.
(110) Park, J.; Lee, K. H.; Galloway, J. F.; Searson, P. C. *J. Phys. Chem. C* **2008**, *112*, 17849.
(111) Piepenbrock, M.-O. M.; Stirner, T.; O'Niell, M.; Kelly, S. M. *J. Am. Chem. Soc.* **2007**, *129*, 7674.
(112) Thessing, J.; Qian, J.; Chen, H.; Pradhan, N.; Peng, X. *J. Am. Chem. Soc.* **2007**, *129*, 2736.
(113) Van Embden, J.; Mulvaney, P. *Langmuir* **2005**, *21*, 10226.
(114) Bullen, C. R.; Mulvaney, P. *Nano Lett.* **2004**, *4*, 2303.
(115) Qu, L.; Yu, W. W.; Peng, X. *Nano Lett.* **2004**, *4*, 465.
(116) Brazeau, A. L.; Jones, N. D. *J. Phys. Chem. C* **2009**, *113*, 20246.
(117) Spanhel, L.; Anderson, M. A. *J. Am. Chem. Soc.* **1991**, *113*, 2826.
(118) Lee, E. J. H.; Ribeiro, C.; Longo, E.; Leite, E. R. *J. Phys. Chem. B* **2005**, *109*, 20842.
(119) Lee, E. J.; Ribeiro, C.; Longo, E.; Leite, E. R. *Chem. Phys.* **2006**, *328*, 229.
(120) Meakin, P. *Annu. Rev. Phys. Chem.* **1988**, *39*, 237.
(121) Wang, H.; Xie, C.; Zeng, D. *J. Cryst. Growth.* **2005**, *277*, 372.
(122) Briois, V.; Giorgetti, C.; Baudelet, F.; Blanchandin, S.; Tokumoto, M. S.; Pulcinelli, S. H.; Santilli, C. V. *J. Phys. Chem. C* **2007**, *111*, 3253.
(123) Pesika, N. S.; Stebe, K. J.; Searson, P. C. *J. Phys. Chem. B* **2003**, *107*, 10412.
(124) Hu, Z.; Escamilla Ramírez, D. J.; Heredia Cervera, B. E.; Oskam, G.; Searson, P. C. *J. Phys. Chem. B* **2005**, *109*, 11209.
(125) Kang, K.; Redner, S.; Meakin, P.; Leyvraz, F. *Phys. Rev. A* **1986**, *33*, 1171.
(126) Stöber, W.; Fink, A.; Bohn, E. *J. Colloid Interface Sci.* **1968**, *26*, 62.
(127) Pontoni, D.; Narayanan, T.; Rennie, A. R. *Langmuir* **2002**, *18*, 56.
(128) Green, D.; Lin, J.; Lam, Y.-F.; Hu, M.-C.; Schaefer, D. W.; Harris, M. J. *J. Colloid Interface Sci.* **2003**, *266*, 346.
(129) Yokoi, T.; Sakamoto, Y.; Terasaki, O.; Kubota, Y.; Okubo, T.; Tatsumi, T. *J. Am. Chem. Soc.* **2006**, *128*, 13664.
(130) Yokoi, T.; Wakabayashi, J.; Otsuka, Y.; Fan, W.; Iwama, M.; Watanabe, R.; Aramaki, K.; Shimojima, A.; Tatsumi, T.; Okubo, T. *Chem. Mater.* **2009**, *21*, 3719.
(131) Hartlen, K. D.; Athanasopoulos, A. P. T.; Kitaev, V. *Langmuir* **2008**, *24*, 1714.
(132) Fouilloux, S.; Désert, A.; Taché, O.; Spalla, O.; Daillant, J.; Thill, A. *J. Colloid Interface Sci.* **2010**, *346*, 79.
(133) Ruckenstein, E.; Djikaev, Y. *Adv. Colloid Interface Sci.* **2005**, *118*, 51.
(134) Yamada, H.; Urata, C.; Higashitamori, S.; Aoyama, Y.; Yamauchi, Y.; Kuroda, K. *ACS Appl. Mater. Interfaces* **2014**, *6*, 3400.
(135) Héloïse, D. P.-S.; Abraham, C.; Céline, C.-B.; Séverinne, R.; Laure, M.; Loïc, V.; and Bénédicte, L. *J. Phys. Chem. C* **2014**, *118*, 4959.
(136) Liu, H.; Owen, J. S.; Alivisatos, A. P. *J. Am. Chem. Soc.* **2007**, *129*, 305.
(137) Reiss, P. *New J. Chem.* **2007**, *31*, 1843.
(138) Yu, K. *Adv. Mater.* **2012**, *24*, 1123.
(139) Szostak, M.; Aubé, J. *Chem. Rev.* **2013**, *113*, 5701.